BCSJ

Award Accounts

The Chemical Society of Japan Award for 2014
The Chemical Society of Japan Award for Young Chemists for 2011

Adaptive Building Blocks Consisting of Rigid Triangular Core and Flexible Alkoxy Chains for Self-Assembly at Liquid/Solid Interfaces

Yoshito Tobe,*[1] Kazukuni Tahara,*[1,†] and Steven De Feyter*[2]

[1]Division of Frontier Materials Science, Graduate School of Engineering Science, Osaka University, 1-3 Machikaneyama, Toyonaka, Osaka 560-8531

[2]KU Leuven-University of Leuven, Department of Chemistry, Division of Molecular Imaging and Photonics, Celestijnenlaan 200F, B-3001 Leuven, Belgium

E-mail: tobe@chem.es.osaka-u.ac.jp, tahara@meiji.ac.jp, Steven.DeFeyter@chem.kuleuven.be

Received: June 14, 2016; Accepted: July 26, 2016; Web Released: August 19, 2016

Yoshito Tobe 【Award recipient】
Yoshito Tobe received his Ph.D. (1979) from Osaka University under the supervision of Professor Y. Odaira. He was appointed as Assistant Professor at Osaka University and was promoted to Lecturer (1983), Associate Professor (1992), and Professor (1998). He was Visiting Professor from 1987 to 1988 with Professor P. E. Eaton at the University of Chicago. He is a recipient of the Chemical Society of Japan Award for Young Chemists for 1984, Society of Synthetic Organic Chemistry Japan Award for 2011, and the Chemical Society of Japan Award for 2014. His current research focuses on exotic aromatic compounds and on-surface supramolecular chemistry.

Kazukuni Tahara 【Award recipient】
Kazukuni Tahara received his B.S. degree from the School of Science and Technology, Meiji University in 2000 and then studied at the Graduate School of Science, The University of Tokyo, obtaining his Ph.D. in 2005 under the direction of Professor Eiichi Nakamura. After postdoctoral work (JSPS research fellow) with Professor Yoshito Tobe at the Graduate School of Engineering Science, Osaka University, he became an assistant professor at the same institute in 2006. He became an associate professor at the School of Science and Technology, Meiji University in 2016. He is a recipient of the Chemical Society of Japan Award for Young Chemists for 2011. His current interests include synthesis of π-conjugated molecules for on-surface self-assembly, and functionalization of graphitic surfaces.

Steven De Feyter
Steven De Feyter has been a full professor since 2011 at KU Leuven—University of Leuven in Belgium. After starting up scanning tunneling microscopy during his Ph.D. in the group of Prof. Frans C. De Schryver at KU Leuven he moved for a postdoctoral position to the group of Prof. Ahmed Zewail (Caltech) where he was involved in ultrafast organic femtochemistry. His current interests include the study of supramolecular chemistry and self-assembly phenomena at surfaces, including modification of 2D materials, with a focus on liquid–solid interfaces. In 2013, he was awarded an ERC advanced grant.

Abstract

Supramolecular self-assembly in two-dimensional (2D) spaces on solid surfaces is the subject of intense current interest because of perspectives for various applications in nanoscience and nanotechnology. At the liquid/graphite interface, we found by means of scanning tunneling microscopy molecules with a rigid triangular core, a twelve-membered phenylene-ethynylene macrocycle called dehydrobenzo[12]-

† Present address: Department of Applied Chemistry, School of Science and Technology, Meiji University, 1-1-1 Higashimita, Tama-ku, Kawasaki, Kanagawa 214-8571

annulene (DBA), substituted by six flexible alkoxy chains self-assembled to form hexagonal porous 2D molecular networks via van der Waals interactions between interdigitated alkyl chains as the directional intermolecular linkages. Factors that affect the formation of the porous 2D molecular networks including alkyl chain length, solvent, solute concentration, and temperature were elucidated through a systematic study. Because DBA molecules are versatile for chemical modification, they turned out to be highly adaptive for on-surface supramolecular chemistry with respect to (i) pore size control by changing the chain length, (ii) study of parity effect due to even or odd number chains, (iii) generation of supramolecular chirality on surfaces by introducing stereocenters, (iv) chemical modification of the pore interior for selective co-adsorption of guest molecules by introducing functional groups. Additionally, formation of superlattice structures on surfaces was incidentally observed by mixing DBAs of different alkoxy chain parity or by addition of guest molecules via an induced-fit mechanism. These results made significant contribution to advancement of supramolecular chemistry in 2D space.

1. Introduction

The control of the spatial organization of functional molecules based on self-assembly plays a central role in organic soft materials such as liquid crystals[1] and gels[2] as well as optoelectronic materials for bulk heterojunction photovoltaics.[3] In particular, among various types of molecular self-assemblies of different structural dimensionality, those in two-dimensional (2D) space on solid surfaces are the subjects of intense contemporary interest because of the prospective applications in the field of nanoscience and nanotechnology.[4] In this context, numerous 2D structures formed by supramolecular self-assembly on surfaces have been reported during the past decades.[5–8] This rapidly advancing research field is called "2D crystal engineering"[7] in analogy with the well-established field known as "crystal engineering" for design and synthesis of molecular crystal structures based on control over intermolecular interactions in three-dimensional (3D) systems.[9]

For the investigation of 2D molecular networks formed by self-assembly of molecules on surfaces, scanning tunneling microscopy (STM) has been used as an extremely powerful tool because of its potential for structural "visualization" with molecular scale precision.[10] STM can be operated under ultra-high vacuum (UHV) conditions or typically at the interface between an atomically flat conducting solid phase and either a gas or liquid phase. Advantages of UHV conditions are a large temperature range enabling stable imaging of molecular networks with high resolution and measurements of electric and magnetic responses of molecules at very low temperatures,[5] and generation at high temperatures of highly reactive intermediates which can survive only under inert atmosphere. However, limitations exist with regard to tolerance to the deposition process by sublimation for thermally unstable molecules of large molecular size. In contrast, at the liquid/solid interface, a wide range of molecules can be used for STM experiments,[11] though the temperature range is relatively narrow (ca. 100 °C). The most advantageous aspect of the liquid–solid interface systems is the dynamic nature due to the existence of a supernatant solution phase that serves as a reservoir of solute molecules, allowing repairing of defects in a molecular network or reorganization of a network structure in response to chemical potentials of the building blocks that depend on variable parameters such as solute concentration and temperature. From these points of view, the formation of 2D molecular networks at the liquid/solid interface has become a prevailing research field.[6–8]

With the above mentioned backgrounds and perspectives in mind, we embarked on a research program on 2D self-assembly at liquid/solid interfaces using molecules with a rigid triangular core, a twelve-membered phenylene-ethynylene macrocycle called dehydrobenzo[12]annulene (hereafter called DBA), substituted by six flexible alkoxy chains, creating porous 2D molecular networks of hexagonal lattices via van der Waals interactions between interdigitated alkyl chains as the directional intermolecular linkages. We initiated the project in a very strong collaboration, which has lasted more than a decade by now, with Professors Frans De Schryver and Steven De Feyter of KU Leuven, with simple alkyl- and alkoxy-substituted DBA derivatives, with a naïve idea of regular tiling using these triangle motifs.[12] The collaboration started naturally because we had had a strong intention to drive our research on in-solution self-assembly to the chemistry in 2D space, and because we had a number of derivatives and congeners of DBA in stock in connection with our research on DBAs as candidates for organic functional molecules of optoelectronic interest[13] However, the choice of DBA as a rigid core of the building blocks turned out to be crucial for the successful research that followed as described in this Account. During the initial stage of the research, we clarified through a systematic study factors that affect formation of the porous 2D molecular networks, such as alkyl chain length, solvent, solute concentration, and temperature. Then we exploited high adaptivity of DBAs for design and synthesis of advanced 2D monolayers taking full advantage of versatility of DBAs for chemical modification. As a result, we found DBAs were adaptive as well as adaptable for (i) pore size control by changing the alkoxy chain length, (ii) study of parity effect by using even or odd number alkoxy chains, (iii) generation of supramolecular chirality on surfaces by introducing stereocenters into the alkoxy chains, (iv) chemical modification of the pore interior for selective co-adsorption of guest molecules by introducing functional groups at the alkoxy chain terminals. Additionally, formation of superlattice structures on surfaces incidentally was observed by mixing DBAs of different alkoxy chain parity or by addition of guest molecules via an induced-fit mechanism. These studies made significant contribution to advancement of supramolecular chemistry in 2D space. In this Account, we describe the chemistry of 2D self-assembly of alkyl- and alkoxy-substituted DBAs at liquid/solid interfaces as outlined in Figure 1a. We will start with the formation of hexagonal 2D molecular networks created at liquid/solid interfaces by self-assembly of DBAs and its controlling factors, followed by the formation of advanced molecular networks realized taking advantage of the adaptivity of DBAs.

2. Controlling Factors for 2D Molecular Networks at Liquid/Solid Interfaces

It has been well documented that the outcome of supramolecular self-assembly at the liquid/solid interface is determined by the interplay of the following non-covalent interactions between the molecule, substrate, and solvent; (i) molecule–molecule, (ii) molecule–substrate, (iii) molecule–solvent, and (iv) solvent–substrate interactions.[6–8] In this respect, the roles played by these interactions in controlling 2D structures are briefly described in this section.

Molecular building blocks are connected on surfaces by non-covalent molecule–molecule interactions, such as hydrogen bonds, metal–ligand coordination bonds, dipole–dipole interactions, and van der Waals interactions. Hydrogen bonds are most frequently employed because of their relatively strong and highly directional bonding, the factors which make the resulting network structure reliable and predictable. Metal–ligand coordination is particularly useful to construct 2D grids typically on metal surfaces under UHV conditions due to its strength and directionality similar to hydrogen bonds. Dipole–dipole interactions between polar functional groups are known to occasionally play a crucial role in controlling self-assembled structures in addition to being a major driving force of assembly. Because van der Waals interactions per small structural unit are weak and unidirectional compared to the aforementioned interactions, in most cases they serve in a cumulative manner for assembly as frequently observed in close-packed lamellar structures of alkane derivatives.

As atomically flat substrates used for the formation of self-assembled monolayers at the liquid/solid interface, graphite and Au(111) are commonly employed because of their ready availability and chemical stability under ambient conditions. In particular, graphite is conveniently used due to its ease in handling. At the organic solvent/graphite interface, the interaction operating between a substrate and a molecule is basically of van der Waals type. Because alkanes are adsorbed favorably to graphite based on epitaxial stabilization by matching of lattice registry between the methylene units along an alkyl chain and the honeycomb lattice of graphite substrate, alkyl substituents are frequently used to stabilize 2D structures formed on graphite surfaces.

At the liquid/solid interface, solvent molecules exert a significant effect on the network structures, because the type of solvents (i.e., polarity and hydrogen-bond formation), concentration, and temperature affect the thermodynamics of the system arising from solvation. Solvent molecules also compete with the solute molecules toward adsorption on the surface; sometimes they are co-adsorbed in a confined space of molecular networks.[14] Mobility of the molecules[15] at the liquid/solid interface due to the adsorption–desorption dynamics may also be affected by solvation and solvent viscosity.[16]

Finally, it should be pointed out that, since most of the STM experiments at the liquid/solid interface are carried out at ambient temperature, the observed 2D structures are not always the thermodynamically most stable ones due to kinetic effects in the network formation. A kinetically favored phase can be transformed into a thermodynamically more stable phase via adsorption–desorption processes, which occasionally occur during the course of STM observation. Annealing treatments which accelerate the dynamics to achieve an equilibrium are sometimes necessary to reach thermodynamically favored phases.

3. Formation of Nanoporous 2D Molecular Networks

Among various types of self-assembled monolayers formed on surfaces, porous 2D molecular networks, so-called nanoporous networks, have attracted a great deal of attention because of their ability to form multi-component 2D nanostructures by accommodation of guest molecule(s) in surface-confined pores (called nanowells) of these networks.[8,17] For example, nanoporous networks can be used to *isolate* a single molecule or a (number-specific) cluster of functional molecules in confined space due to change in the size, shape, and chemical environment of the porous space. Controlling their optical or electrical properties depending on condition- or stimulus-dependant change in their orientation or mobility would lead to high density data storage systems. Moreover, if the interior is properly functionalized, nanowells may serve not only as templates for precise molecular recognition that can find sensory applications, but also as nanoreactors for catalytic chemical transformations that take place in an efficient and selective manner by combining substrate molecules in confined space similar to biological processes.

The main driving force for co-adsorption of guest molecules in a nanoporous network is the guest–substrate interaction. In addition, shape and size complementarity between the guest and the surrounding host matrix plays an important role in determining the geometry and mobility of the guest due to van der Waals interactions between them. Guest molecules having various shape and size were immobilized in nanoporous networks according to this concept.[18] Moreover, in the recent past, modification of the chemical environment of the interior space for guest binding through specific chemical interactions was reported.[19] Since the nanoporous networks formed by DBAs (Figure 1) were expected to provide a suitable ground for control of guest molecules by size, shape, chirality, and functionality, we put special emphasis on this respect as detailed in this Account.

4. Formation of Porous Networks by Self-Assembly of DBAs with Flexible Alkoxy Chains at Liquid/Solid Interfaces

Our initial experiments on the formation of 2D molecular networks were conducted using alkyl-substituted **DBA-C10** at the 1,2,4-trichlorobenzene (TCB)/graphite interface at relatively high solute concentration of ca. $5–8 \times 10^{-4}$ mol L^{-1} at room temperature (typically 22–24 °C). Fortunately, a porous 2D network with a honeycomb structure was observed as shown in Figure 2 under the conditions (i.e., high solute concentration) which turned out afterwards not ideal for porous structure formation.[20] The bright triangle features are assigned to DBA cores because of the larger tunneling current typically observed for aromatic compounds than for alkanes.[21] Six alkyl chains per **DBA-C10** imaged as bright dots are adsorbed on the surface and they align parallel to one of the graphite's symmetry axes. Therefore, the DBA cores are linked by four alkyl chains which are interdigitated other to maximize van der

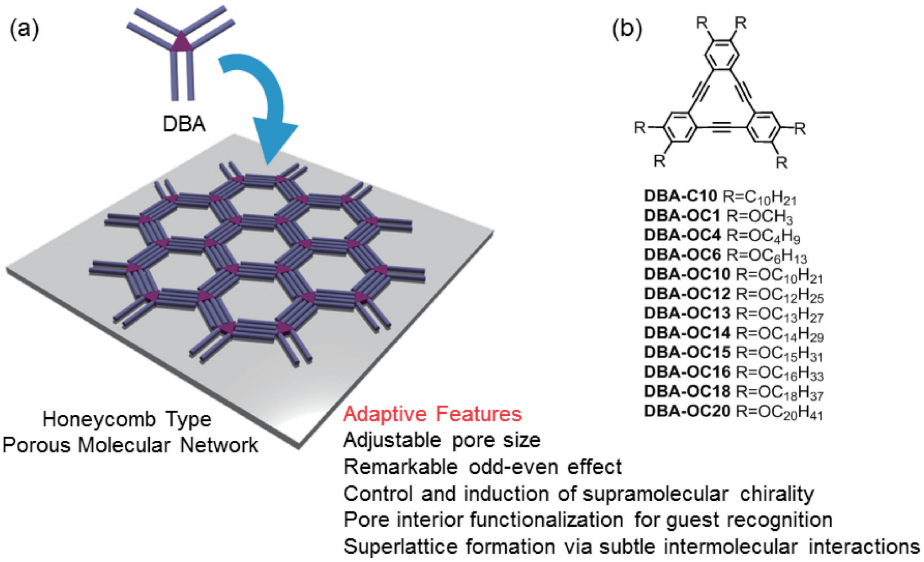

Figure 1. (a) Schematic representation for the formation of a porous molecular network by self-assembly of DBA molecules on a surface and their adaptive features. (b) Chemical structures of simple, so-called first-generation DBA molecules.

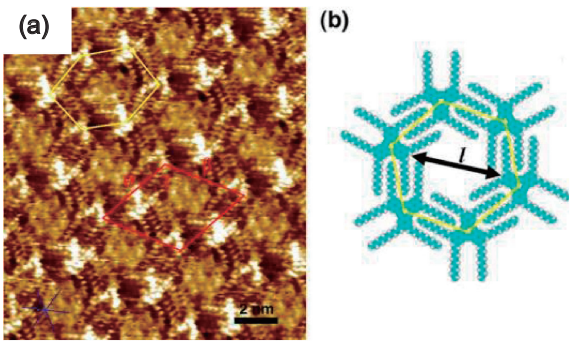

Figure 2. (a) STM image of the molecular network of **DBA-C10** formed at the TCB/graphite interface. The unit cell and main symmetry axes of graphite are indicated by the red lines and the blue lines at the lower left corner, respectively. (b) Molecular model of the honeycomb structure of **DBA-C10**. Reprinted with permission from Ref. 20b. Copyright 2006 American Chemical Society.

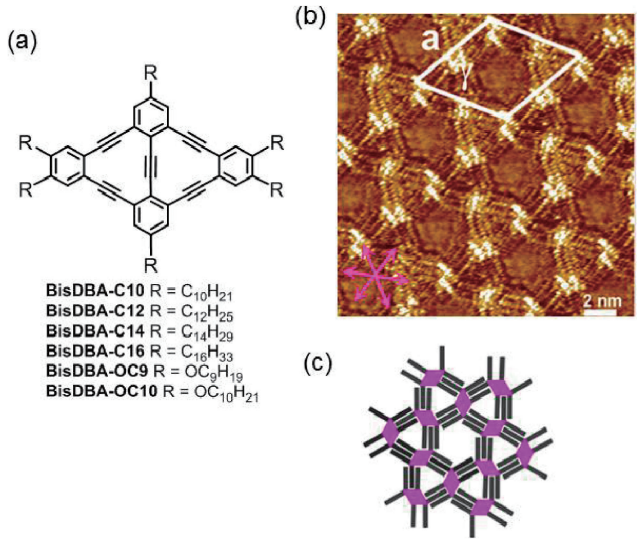

Figure 3. (a) Chemical structures of bisDBAs, **bisDBA-C10** to **bisDBA-C16** and **bisDBA-OC9** and **bisDBA-OC10**, (b) STM image of the Kagomé network formed by **bisDBA-C10** at the TCB/graphite interface, and (c) its model. Reprinted with permission from Ref. 22. Copyright 2009 American Chemical Society.

Waals interactions. In the hexagonal pores fuzzy (typically seven) dim spots are observed, which we ascribe to co-adsorbed solvent (TCB) molecules. Following the initial lucky outcome with **DBA-C10**, we found that alkoxy-substituted DBAs, which were more readily prepared than the alkyl derivatives, with alkoxy groups ranging from OC_4H_9 (**DBA-OC4**, Figure 1) to $OC_{20}H_{21}$ (**DBA-OC20**, Figure 1) also formed hexagonal lattices, revealing it is a general phenomenon of alkoxy DBAs to form nanoporous networks. However, by systematic investigations on the self-assembling behaviors of alkoxy-substituted DBA derivatives under various experimental conditions, we found that the self-assembled monolayer patterns were significantly affected by the structure of the triangular building blocks, such as the size of the rigid core and the flexible alkyl chain length, as well as experimental conditions including solvent, concentration, temperature, and the solid substrates, as described in the following sections.

In addition to **DBA-C10**, we found that **bisDBA-C10** with two DBA cores fused to a common edge formed a porous Kagomé network having hexagonal and triangle pore spaces at the TCB/graphite interface (Figure 3).[20a,22] Because the bisDBA core is connected to four neighbor molecules by six alkyl chains, each intermolecular linkage is formed by three alkyl chains, in contrast to the case of the honeycomb network of **DBA-C10** which is connected by four alkyl chains. This makes the porous Kagomé networks of bisDBA derivatives less efficient as described later in section 4.3.

4.1 Effect of Triangular Core Size on the Formation of Nanoporous Networks. First, by comparison with other alkoxy-substituted triangular molecules, we found that the size of the triangular core is critical to the formation of porous networks due to the distance-dependence between the alkoxy

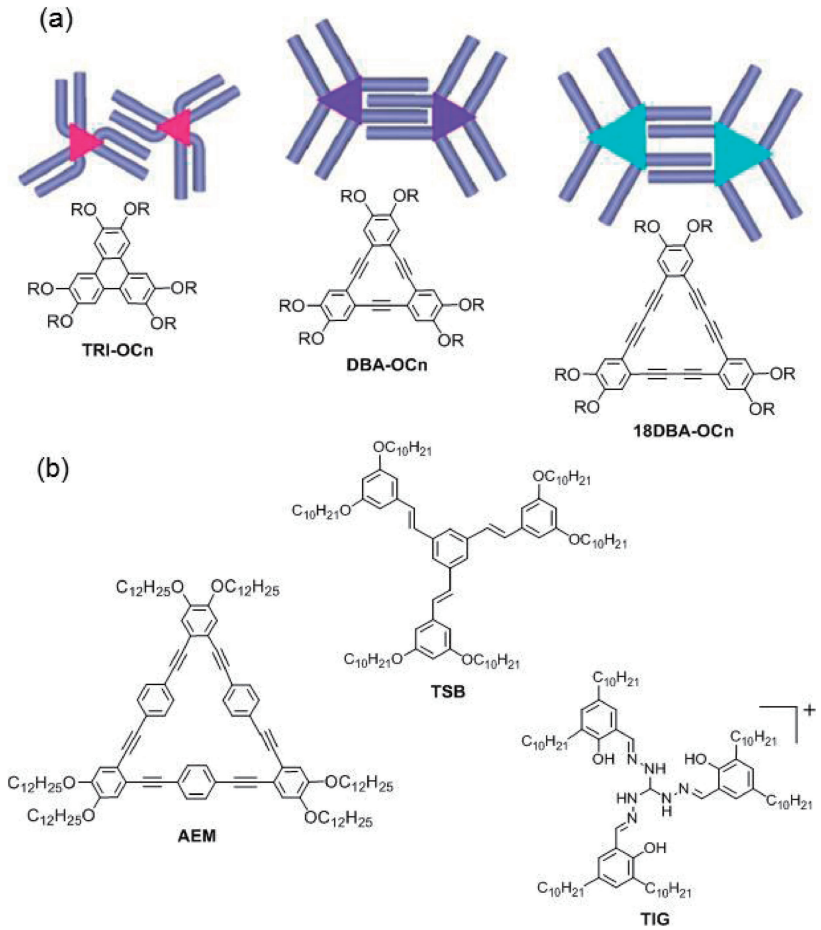

Figure 4. (a) A schematic representation for the effect of core size on alkyl chain interactions with chemical structures of **TRI-OCn**, **DBA-OCn**, and **18DBA-OCn**. (b) Chemical structures of **AEM**, **TSB**, and **TIG**. Reprinted with permission from Ref. 26. Copyright 2007 American Chemical Society.

chains for van der Waals interactions. The theoretically estimated ideal distance for two parallel-aligned chains which are placed on a graphite surface to maximize van der Waals interaction is reported to be 0.49 nm.[23] Experimentally observed distances range typically from 0.40 to 0.45 nm.[11,24] Hence the optimal distance between a pair of alkyl chains attached to a rigid core of a molecule to form a van der Waals linkage with its partner molecule should be 0.98 nm. Because the distance between the alkoxy chains (O–O distance of 0.98 nm) of alkoxy-substituted DBAs falls into this criterion, they are inherently suited for the porous network formation (Figure 4a). On the other hand, it had been reported by Bai and co-workers that triphenylene derivatives **TRI-OCn** (alkyl chain: $C_{10}H_{21}$, $C_{12}H_{25}$, $C_{14}H_{29}$, $C_{16}H_{33}$), in which the distance between alkoxy chain (O–O distance) is 0.73 nm, formed close-packed hexagonal or linear type monolayers through van der Waals interactions between alkyl chains.[25] No porous pattern was formed, because the distance between alkoxy chains is too small to allow them being interdigitated. For a larger triangular core, we found that alkoxy-substituted dehydrobenzo[18]annulenes such as **18DBA-OCn** (alkyl chain: $C_{10}H_{21}$, $C_{12}H_{25}$, $C_{14}H_{29}$, $C_{16}H_{33}$), in which the alkoxy chain distance is 1.24 nm, did not form honeycomb patterns at the TCB/graphite interface, because the alkoxy chain distance was too large for stable interdigitation.[26]

Recently, Zhao, Lei, and co-workers reported that arylene-ethynylene macrocycles with even larger triangular core such as **AEM** (Figure 4b) behaved similarly; depending on the concentration, different types of non-porous networks were observed at the TCB/graphite interface.[27]

The above consideration also applies for the formation of porous networks by trigonal building blocks with six alkoxy chains (Figure 4b). Namely, at the same time as our initial finding for the formation of honeycomb network, Charra, Atias, and co-workers reported the porous network formation by alkoxy-substituted 1,3,5-tristyrylbenzene derivative **TSB** at the 1-phenyloctane/graphite interface.[17b,28] Moreover, we recently found that trigonal triiminoguadinium salt **TIG** with C10 alkoxy chains formed a honeycomb network at the 1-phenyloctane/graphite interface.[29a] In **TSB** and **TIG**, the distances between the alkoxy chains are estimated from the theoretically optimized models to be 1.15 and ca. 1 nm, respectively, in accordance with the empirical rule elucidated from the triangular building blocks. Recently, Matsuda and Hirose reported the formation of a honeycomb network by self-assembly of a hexaalkoxy-substituted compound with a sulfur-containing tetracyclic core, which was generated by photoisomerization of a diarylethene precursor,[29b] supporting the above guideline for formation of porous networks by alkyl chain interdigitation.

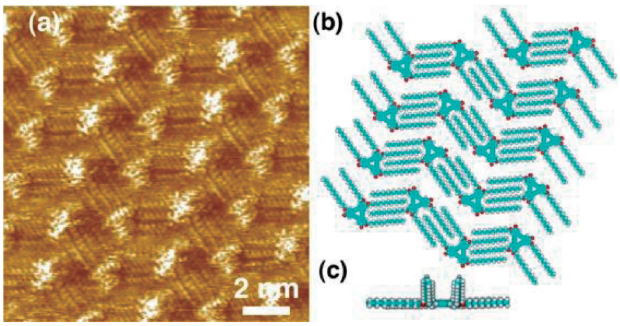

Figure 5. (a) High-resolution STM image of the non-porous network of **DBA-OC14** at the TCB/graphite interface. (b) Top view and (c) side view of its model. Two alkyl chains per molecule are omitted for clarity in (b). Reprinted with permission from Ref. 20b. Copyright 2006 American Chemical Society.

4.2 Effect of Alkyl Chain Length on the Formation of Nanoporous vs. Non-porous Networks. In contrast to **DBA-C10** which formed a porous 2D pattern even at concentrations higher than 10^{-4} mol L^{-1} at room temperature, alkoxy-substituted DBAs were found to exhibit both or either of the porous honeycomb and/or non-porous patterns depending on the alkoxy chain length under similar conditions.[20b] Whereas **DBA-OC10** having decyloxy side chains forms a honeycomb network similar to **DBA-C10**, **DBA-OC12** exhibited domains of the non-porous structure in addition to the honeycomb structure. The tendency to form the non-porous structure increases with increasing alkoxy chain length. Thus, while **DBA-OC14** formed non-porous domains mainly with some honeycomb structures observed at the domain boundaries, for **DBA-OC16** and **DBA-OC18**, the non-porous networks were predominantly observed. In addition, with increasing alkyl chain length, the domain size of the non-porous pattern becomes smaller. A high-resolution image of **DBA-OC14** shown in Figure 5 clearly shows the presence of four interdigitated alkyl chains between the DBA cores, indicating that the other two alkyl chains attached to the DBA core are not adsorbed on the graphite surface and are exposed to the solution phase.

4.3 Effect of Concentration on the Formation of Nanoporous vs. Non-porous Networks: A Semiquantitative Thermodynamic Analysis. The formation of non-porous structures for DBAs with long alkyl chains seemed to set a limitation to further advance of this chemistry. To our delight, however, we found that the network structures could be changed dependent on the concentration of DBAs in TCB; by diluting the concentration, the dominant network structures turned to the porous phase.[30] For example, as sown in Figure 6, whereas **DBA-OC16** showed exclusively the close-packed network at 1.1×10^{-4} mol L^{-1}, the network structure changed almost completely to the porous honeycomb type at 5.7×10^{-6} mol L^{-1}. This concentration dependent behavior turned out to be general for all DBA derivatives.

The concentration range of this transition from the non-porous to porous patterns depends on the alkyl chain length, as shown in Figure 7 for **DBA-OC12** to **DBA-OC18**. Whereas **DBA-OC12** formed exclusively the honeycomb structure even at 2×10^{-4} mol L^{-1}, the network structure of **DBA-OC18**

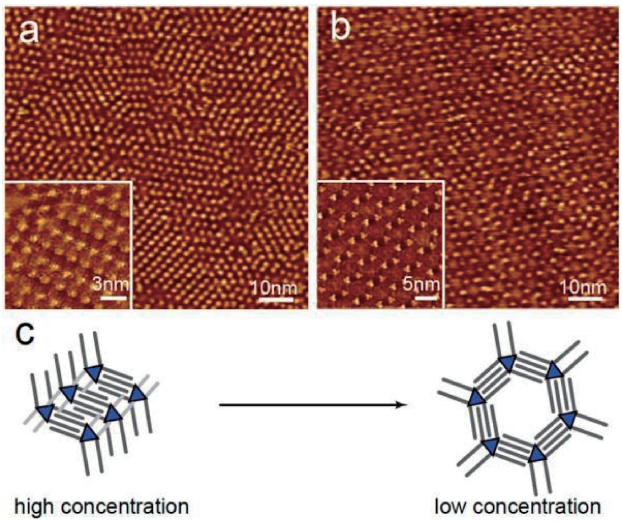

Figure 6. (a, b) STM images obtained at the TCB/graphite interface of monolayers formed by **DBA-OC16** at concentrations (a) 1.1×10^{-4} mol L^{-1} and (b) 5.7×10^{-6} mol L^{-1}. Insets in (a) and (b) are high-resolution images of the non-porous and honeycomb patterns, respectively. (c) A scheme illustrating the structure transition from the non-porous to honeycomb patterns. Reprinted with permission from Ref. 30. Copyright 2008 John Wiley and Sons.

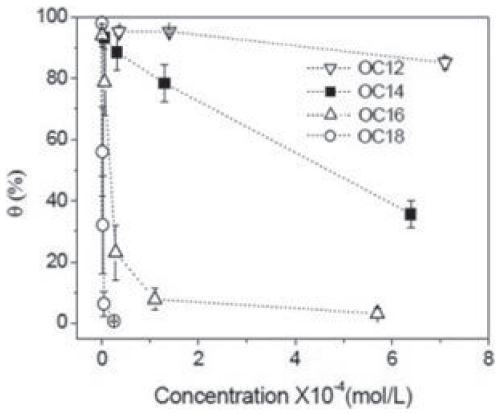

Figure 7. Dependency of the coverage θ (%) of the honeycomb versus close-packed linear structures formed at the TCB/graphite interface on the DBA concentration. Reprinted with permission from Ref. 30. Copyright 2008 John Wiley and Sons.

changed to the honeycomb pattern at concentrations of a 10^{-6} mol L^{-1} level. This dilution method for the formation of porous structures was also applicable to **DBA-OC20** which formed exclusively the honeycomb pattern at 2.4×10^{-6} mol L^{-1}. However, while **DBA-OC30** exhibited the porous honeycomb network at the lowest concentrations examined (5.0×10^{-6} mol L^{-1}), dense-packed non-porous structures also co-existed, setting the size limit of the nanoporous networks that can be constructed from the alkoxy-substituted DBAs.[31] This limitation was overcome by introduction of geometrical kinks by inserting a diacetylene unit, which served like a harness to bind long alkyl chains, at proper positions in the alkyl chain as in **DBA-DAOC24OC25** and **DBA-DAOC32OC33** (Figure 8).[32] **DBA-DAOC24OC25** formed relatively large domains of the

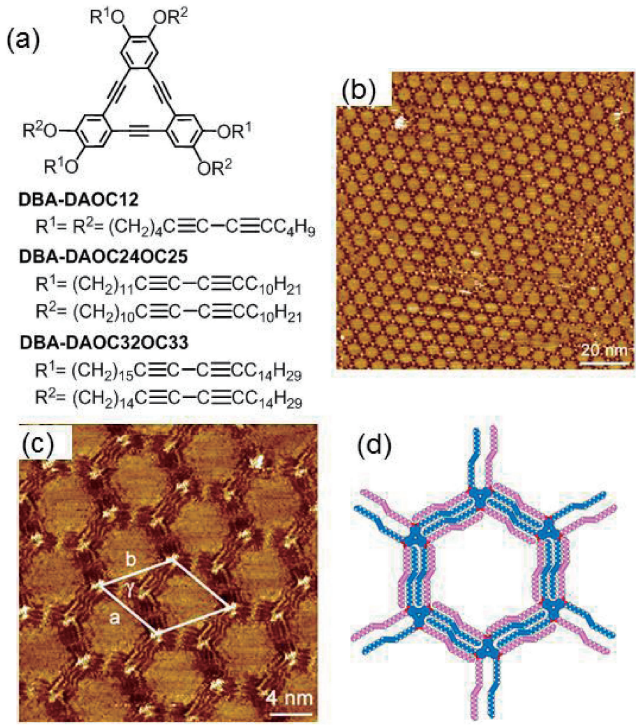

Figure 8. (a) Chemical structures of DBAs bearing diacetylene units inserted in the alkyl chains. (b, c) STM images of a monolayer formed by **DBA-DAOC24OC25** at the TCB/graphite interface. (d) A network model for a honeycomb structure of **DBA-DAOC24OC25**. Reproduced from Ref. 32 with permission from The Royal Society of Chemistry.

honeycomb pattern with a pore size larger than that of **DBA-OC20**. The diacetylene units can be visualized as bright features making kinks in the alkyl chain linkages (Figure 8c). Though the pore size of the network of **DBA-DAOC32OC33** becomes even larger, the size of regular domains becomes smaller. It should be pointed out that the length of the alkyl chains connecting the DBA core and the diacetylene unit are different by one methylene unit in an alternating fashion to make the diacetylene units align favorably. This elaborate molecular design is crucial for the formation of porous structures, because **DBA-DAOC12** bearing the same C6 methylene units between the DBA core and the diacetylene unit did not form an ordered monolayer. Selective synthesis of alternately substituted DBA derivatives is described later in section 5.3 (Scheme 1).

The concentration dependence of the 2D networks of DBAs can be qualitatively explained in terms of the different stabilities and molecular densities between the two phases. Namely, the adsorption energies per unit area for the non-porous phase will become more favorable with increasing alkyl chain length. As the concentration decreases, however, the number of molecules that cover the substrate surface decreases. Consequently, at low concentrations (a 10^{-6} mol L^{-1} level or lower) DBAs prefer to form a porous honeycomb structure of lower density to maximize the adsorption energy per molecule. This trend becomes more remarkable for DBAs with short alkoxy chain length because of the increasing stability difference between the porous honeycomb structures.

The concentration dependent change of the network pattern was also observed for bisDBAs (Figure 3), although it was more complicated because of the weaker intermolecular binding force between the rhombus cores. While **bisDBA-C10** exclusively forms the Kagomé structure for a wide concentration range (from 10^{-4} to 10^{-6} mol L^{-1}), **bisDBA-C12** to **bisDBA-C16** with longer alkyl chains form a variety of concentration dependent structural variations.[22] Moreover, alkoxy-substituted **bisDBA-OC9** and **bisDBA-OC10** with C9 and C10 alkoxy chains, respectively, never formed the Kagomé patterns, indicating the delicate structural requirement for stable van der Waals pairs.

The control of dense-packed vs. porous network patterns at the liquid/solid interface by solute concentration is related to the known structural control by surface coverage under ultrahigh vacuum conditions.[33] Because of the facility of structural control in the liquid/solid interface system as well as the interest in the role of solvent, the solute concentration control method was quickly recognized in this field and it became a common practice. A number of examples of concentration-dependent control for the 2D networks formed by hydrogen bonding were reported,[34] including a binary system of 1,3,5-benzenetricarboxylic acid (trimesic acid, **TMA**) and 1,3,5-tris-(4-carboxylphenyl)benzene at the liquid/solid interfaces to take just one example.[34a] All reported results are consistent with our view; the lower the concentration, the larger the chance to find a low density pattern.

The above results on the effect of concentration on the non-porous vs. porous packing patterns prompted us to understand thermodynamics of 2D self-assembly at interfaces by quantitative analysis.[35] We therefore carried out an analysis of the stabilities of different monolayer network patterns formed at the TCB/graphite interface by **DBA-OC10**–**DBA-OC18**.[30] By taking into account the number of DBA molecules per unit area (h and l for the porous honeycomb and non-porous linear patterns, respectively) and assuming that the chemical potentials of a DBA molecule in the honeycomb pattern, linear pattern, and in solution are equal, a linear relationship between $\ln(Y_h/[\mathrm{DBA}])$ versus $\ln\{(1-Y_h)/[\mathrm{DBA}]\}$ was elucidated (eq 1), where Y_h is the fraction of the monolayer area occupied by the honeycomb pattern ($Y_h + Y_l = 1$, Y_l: fraction of the monolayer area occupied by the non-porous linear pattern). The slope m is the ratio (l/h) of the packing densities of the linear and the honeycomb patterns and [DBA] is the solute concentration.

$$\ln\left(\frac{Y_h}{[\mathrm{DBA}]}\right) = m\ln\left(\frac{1-Y_h}{[\mathrm{DBA}]}\right) + \ln K \quad (1)$$

The slope m obtained from the experimental data (linear fits by solid lines) in Figure 9a increases with increasing alkyl chain length (solid squares with a solid line, Figure 9b), in agreement with that derived from the packing densities estimated from the molecular models (dotted line, Figure 9b). The intercept $\ln K$ in eq 1 is an equilibrium constant for the transition from the non-porous to honeycomb phases and it shows a linear dependency on the alkyl chain length (circles with a solid line, Figure 9b), also consistent with the monotonic change upon increasing the alkyl chain length. The concentration dependency of the self-assembly of DBAs is thus semi-quantitatively explained in terms of the different stability

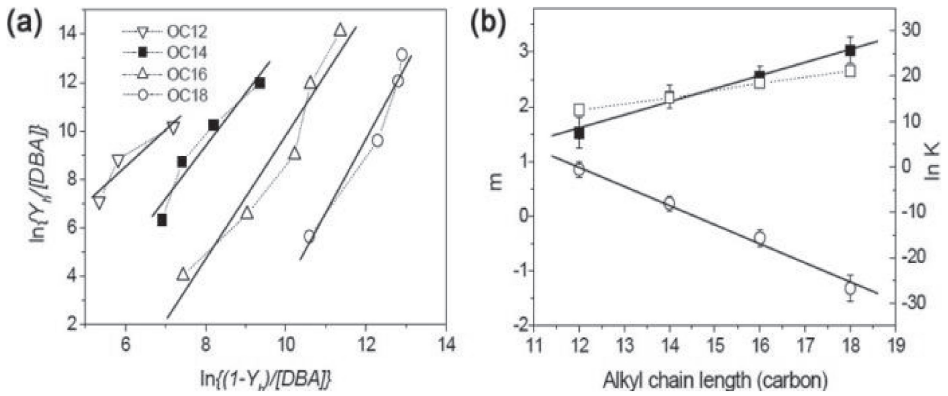

Figure 9. (a) Experimentally obtained plots of $\ln(Y_h/[DBA])$ versus $\ln\{(1 - Y_h)/[DBA]\}$. The solid lines are linear fits. (b) The dependency of slope m (■ experimental; □ estimated from the area per unit cell) and intercept $\ln K$ (○) in eq 1 on the alkyl chain length. The solid lines are linear fits of m and $\ln K$. Reprinted with permission from Ref. 30. Copyright 2008 John Wiley and Sons.

and molecular density of the two network patterns. Moreover, the larger energy difference between the network patterns leads to higher sensitivity to concentration.

4.4 Effect of Temperature on the Formation of Porous vs. Non-porous Networks: A Thermodynamic Model for 2D Assembly at Liquid/Solid Interfaces. As described above, we revealed the concentration effect on the 2D self-assembly patterns of DBAs at room temperature and proposed a semi-quantitative thermodynamic model. It has been known that 2D self-assembly often displays transitions between phases in response to temperature too,[34b,36] and a few simple thermodynamic models have been developed to describe such systems.[30,34b,37] However, no enthalpy or entropy changes associated with phase transition in 2D self-assembly have been reported. By using the reversible transition between the non-porous and porous phases of **DBA-OC16** at the TCB/graphite interface, we performed the first investigation of the temperature-concentration-dependent structural transition in a 2D self-assembly process. The experimental conditions were selected because the phase transition took place at a measurable temperature range within an experimental concentration range. On the basis of the detailed STM observations, experimentally measured values for enthalpy and entropy changes for the structural transition were elucidated and the experimental enthalpy and entropy values were compared with those obtained from molecular mechanics (MM) simulations and theoretical calculations.

Figures 10a–10f show STM images for sequential heating of **DBA-OC16** at the TCB/graphite interface (5.8×10^{-4} mol L^{-1}) from 22 to 80 °C. At 22 °C the predominantly formed network was the non-porous phase with small domains with width of 5 to 20 nm (Figure 10a). Heating up to 60 °C induced increase of domain size to 50–200 nm, via a process reminiscent of 2D Ostwald ripening by which a system evolves to minimize energetically unfavorable domain boundaries. Similar results were reported for various 2D supramolecular networks[39] including the one for a similar molecule by Bellec et al.[37a] At ca. 70 °C a structural change occurred, forming lines of porous structures with a width of one hexagonal pore within domains of the linear non-porous phase (Figure 10d). By heating to 80 °C complete transition to large domains of the porous phase was observed (Figure 10e). When the system was allowed to cool naturally to 30 °C, a transition back to the linear non-porous phase was observed (Figure 10f). By repeating this heating and cooling process, the system underwent the phase transition multiple times.

The temperature-dependent phase transition behavior of **DBA-OC16** was concentration dependent. Some of the results of the sequential heating experiments at concentrations between 2.30×10^{-5} mol L^{-1} and 2.87×10^{-4} mol L^{-1} are shown in Figure 11a with sigmoidal fits to the experimental data. At lower concentrations, the transition became more gradual and shifted to lower temperatures. Based on the thermodynamic model proposed by Bellec and co-workers for the phase transition occurring at a single critical concentration (C_0),[37a] we derived eq 2 with the addition of a term to model the entropy loss associated with the co-adsorption of solvent molecules. At C_0 the change in free energy going from the non-porous linear to porous honeycomb phases per unit area is equal to zero.

$$\ln C_0 = \frac{1}{T_0}\left(-\Delta H^0_{lin} + \frac{(\Delta H^0_{por} - \Delta H^0_{lin})}{(m-1)}\right) + \Delta S^0_{lin} - \frac{(\Delta S^0_{por} - \Delta S^0_{lin})}{(m-1)} - \frac{19\Delta S^0_{TCB}}{2(m-1)} \quad (2)$$

In eq 2, ΔH^0_{lin} and ΔH^0_{por} are the enthalpy change per DBA molecule for desorption from the surface in the non-porous linear and porous honeycomb phases, respectively, due to molecule–substrate, molecule–molecule and molecule–solvent interactions. ΔS^0_{lin} and ΔS^0_{por} are the entropy changes per DBA associated with desorption from the non-porous and porous phases, respectively, and ΔS^0_{TCB} is the entropy change per TCB molecule for desorption from the surface. The factor of 19/2 in eq 2 is based on the 19 TCB molecules, estimated by both modeling and STM observation, and 6 DBA molecules per pore in the porous structure. Since each DBA is shared by three adjacent pores, the number of TCB per DBA is 19/2. The parameter m is the ratio of surface molecular densities of DBA in the porous and non-porous phases. Equation 2 is based on the fact that at C_0 the enthalpy cost of converting the non-porous phase into the porous phase per unit area is exactly offset by the gain in entropy.

Equation 2 also indicates that C_0 is temperature dependent. A plot of $\ln(C_0)$ against $1/T_0$ (T_0: phase transition temperature

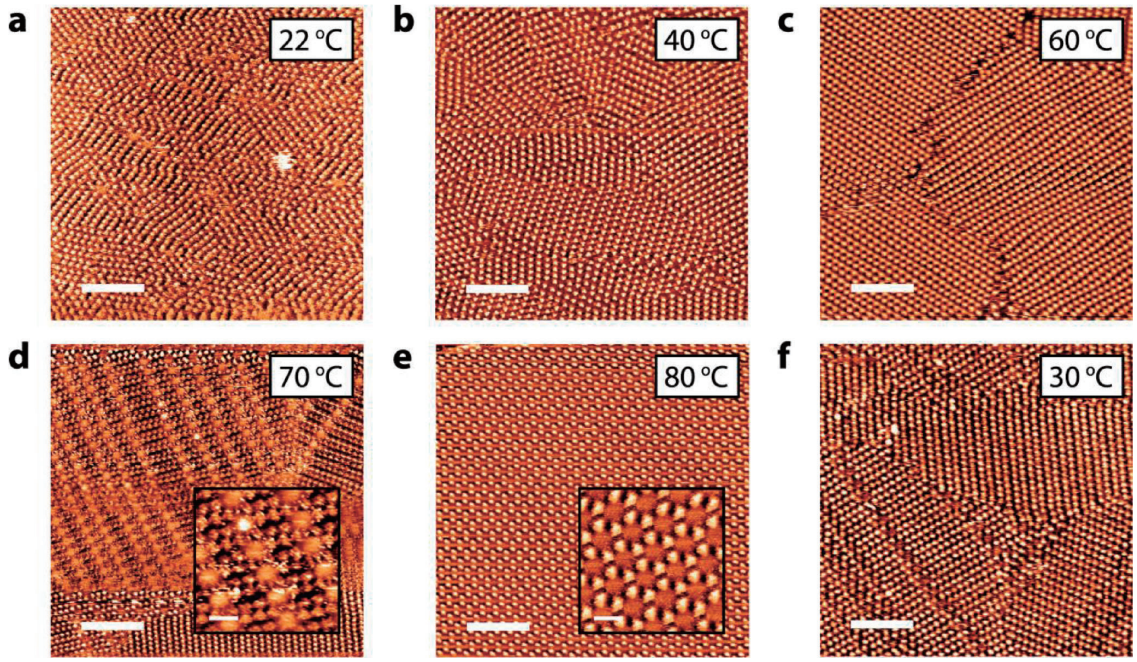

Figure 10. Typical STM images for a sequential heating experiment for a TCB solution (5.8×10^{-4} mol L^{-1}) of **DBA-OC16** at the interface of graphite. After initial deposition of the solution on the substrate at 22 °C, the temperature was increased in 10 °C steps and STM images were collected at each temperature. Images obtained at (a) 22, (b) 40, (c) 60, (d) 70, and (e) 80 °C. (f) STM image after the system was allowed to cool to 30 °C after heating at 80 °C. The insets in (d) and (e) show enlarged regions of the DBA networks. Scale bars; (a), (b), and (c) 16 nm; (d), (e), and (f) 20 nm; insets in (d) and (e) 4 nm. Reprinted with permission from Ref. 38. Copyright 2013 American Chemical Society.

defined as the temperature where 50% transition took place) gave a straight line (Figure 11b) by using the values for T_0 and C_0 obtained from the sequential temperature-dependence experiments at various concentrations (Figure 11a). From a linear fit to this data we obtained the slope and intercept to give eqs 3 and 4 for enthalpy and entropy terms, respectively.

$$-\Delta H^0_{lin} + \frac{(\Delta H^0_{por} - \Delta H^0_{lin})}{(m-1)} = -2.57 \pm 0.16 \times 10^{-19}\,\mathrm{J} \tag{3}$$

$$\Delta S^0_{lin} - \frac{(\Delta S^0_{por} - \Delta S^0_{lin})}{(m-1)} - \frac{19\Delta S^0_{TCB}}{2(m-1)} = 6.38 \pm 0.48 \times 10^{-22}\,\mathrm{J\,K^{-1}} \tag{4}$$

To test the validity of these experimental results, MM simulations were performed to calculate ΔH^0_{lin} and ΔH^0_{por}, yielding the enthalpy term of -1.78×10^{-18} J, which was outside the error of the experimental value (eq 3). This difference may result because the MM simulations do not include the bulk solvent layer. The entropy change due to the loss of translational, rotational, conformational, and vibrational entropy was estimated using a method reported by Whitesides and co-workers,[40] to produce a theoretical estimate for the entropy term of $-1.24 \pm 0.16 \times 10^{-21}\,\mathrm{J\,K^{-1}}$. This estimated value has the opposite sign of the experimental value (eq 4) and lies well outside of it. The discrepancy between theory and experiment may be due to the fact that not all molecules including TCB lose entropy on adsorption, though the estimated values assume a complete restriction of molecular motion for all molecules adsorbed on the surface. The experimental and theoretical enthalpy values both suggest that the enthalpy change for the phase transition from the non-porous to porous phases is positive. Since a transition with a positive change in enthalpy is favored if the corresponding change in entropy is also positive, the experimental value for the entropy change is more accurate and relevant than the theoretical estimate.

4.5 Effect of Solvent on the Formation of Porous vs. Non-porous Networks. The results described above were obtained exclusively using TCB as a solvent, which was suited for the formation of the porous pattern presumably due to its strong tendency to co-adsorb and fill the nanoporous space as described in the thermodynamic analysis. However, it has been well known that the solvents exert significant effect on the structures of self-assembled monolayers. It was indeed the case for the 2D networks of DBAs formed at solvent/graphite interfaces. For example, in aromatic solvents (TCB and PO), **DBA-C10** and **bisDBA-C10** formed mainly the honeycomb and Kagomé structures, respectively, which are thermodynamically favorable equilibrium structures because of fast dynamics due to large solvophilicity. Actually, phase transitions were sometimes observed during STM measurements of **DBA-C10** in 1-phenyloctane and **bisDBA-C10** in TCB at room temperature. On the other hand, in octanoic acid (OA) different network structures were observed.[20b] We assume that due to the solvophobic effect and high viscosity of OA, the movement of molecules in the network forming process is slower, leading to kinetically trapped structures.

In addition to the solvophobic/solvophilic effect, solvent molecules are co-adsorbed on the surface at confined spaces formed by self-assembly of DBAs, leading to unique network patterns. As a remarkable example, we found that when tetra-

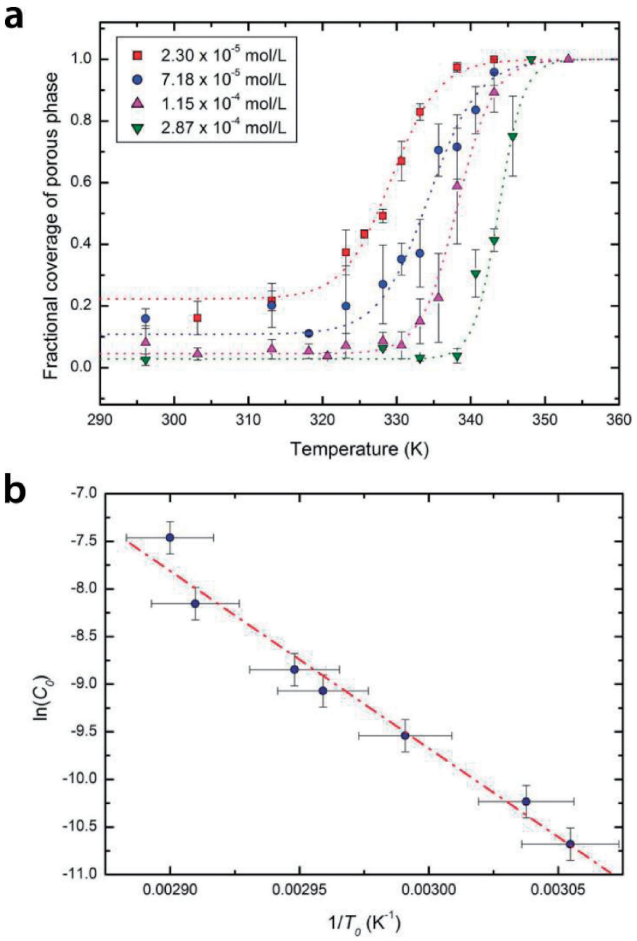

Figure 11. (a) Plots of the fractional coverages of the porous phase as a function of temperature for **DBA-OC16** in TCB at concentrations ranging from 2.30×10^{-5} to 2.87×10^{-4} mol L^{-1}. The dashed lines represent sigmoidal fits to the data. The transition temperature (T_0) is measured by taking the temperature at which the sigmoidal fit equals a fractional coverage of 0.5. (b) Plot of $\ln C_0$ against $1/T_0$ for DBA concentrations between 2.30×10^{-5} and 5.75×10^{-4} mol L^{-1}. The dashed red line represents a linear fit to the data. Reprinted with permission from Ref. 38. Copyright 2013 American Chemical Society.

decane (TD) was used as the solvent, the solvent molecule was incorporated between the two alkyl chains of a DBA, most efficiently in the case of **DBA-OC16** whose alkyl chain length matches that of TD, thereby blocking the intermolecular linkage between the DBA molecules.[41] As a result, domains consisting of linearly aligned molecular rows were observed mainly (Figure 12a). In this structure, two of the three-paired alkyl chains of a DBA molecule are blocked by incorporation of TD molecules, whereas the third alkyl chain pair forms an intermolecular linkage to a neighboring DBA molecule to form a dimer (Figure 12b). Additional tetradecane molecules occupy the open spaces. Moreover, rows consisting of a hexagonal structure which was formed by cooperation of six DBAs and TD molecules occupying every open space were observed at domain boundaries (Figure 12c). A statistical analysis of the numbers of the interdigitated and blocked alkyl chain pairs of DBAs indicate that TD molecules block a significant proportion (63%) of the alkyl chain interdigitation of **DBA-OC16** in contrast to 11% or less proportion for **DBA-OC13**, **DBA-OC14**, and **DBA-OC15**, revealing the delicate balance between the alkyl chain lengths.

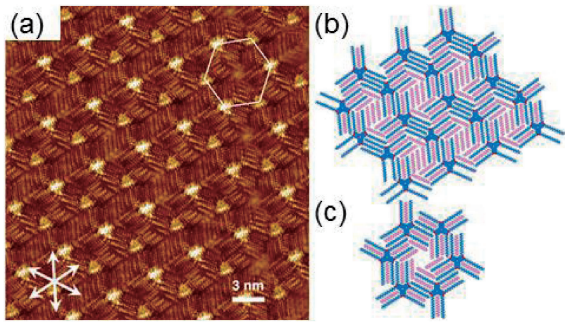

Figure 12. (a) STM image of a monolayer consisting of **DBA-OC16** and tetradecane molecules at the tetradecane/graphite interface (1.0×10^{-6} mol L^{-1}). The hexagonal structure is highlighted by a white hexagon. (b, c) Models of the domains consisting of linearly aligned molecular rows and the hexagonal structure, respectively. Reprinted with permission from Ref. 41. Copyright 2013 American Chemical Society.

4.6 Effect of Substrate on the Structure of 2D Networks. Formation of physisorbed, self-assembled monolayers on graphene has attracted a great deal of interest in view of modification of its unique electronic and mechanical properties.[42] Various kinds of organic molecules have been reported to self-assemble on graphene under UHV conditions.[43] We revealed that the above mentioned porous molecular networks of DBAs can also be formed at the solvent/graphene interface.[44] For example, **DBA-DAOC24OC25** formed a large porous network at the interface between epitaxial few-layer graphene grown on SiC or CVD-grown single-layer graphene on polycrystalline Cu film on silicon wafer and TCB as shown in Figure 13. It should be pointed out that the monolayer continuously crosses the surface steps without structural disorder, exhibiting the adaptability of the molecular network (Figures 13a and 13b). Moreover, it smoothly spreads over the winding surface due to underlying polycrystalline Cu film (Figure 13c). In addition to the formation of the porous networks at the interface of TCB and graphite or graphene, we also found that the supernatant solvent could be removed by simply rinsing the sample gently in water followed by blowing nitrogen to dryness. Thus formed dry monolayers were proven by STM and AFM measurements to retain a highly ordered pattern without obvious defects generated during the drying process. The dried monolayer could be kept for at least two weeks without damage, revealing the stability and robustness of the network in air.[44]

It has been well documented that the solid substrates affect the structures of self-assembled monolayers formed at liquid/solid interfaces.[45] For an alkoxy triphenylene derivative, Charra reported the formation at the tetradecane/Au(111) interface of a close-packed phase which was different from that observed at the solvent/graphite interface under the same conditions.[28,45a] The formation of the different structures was attributed to the mismatch of registry with respect to the Au(111) lattice, in contrast to the solvent/graphite interface in which all six alkyl

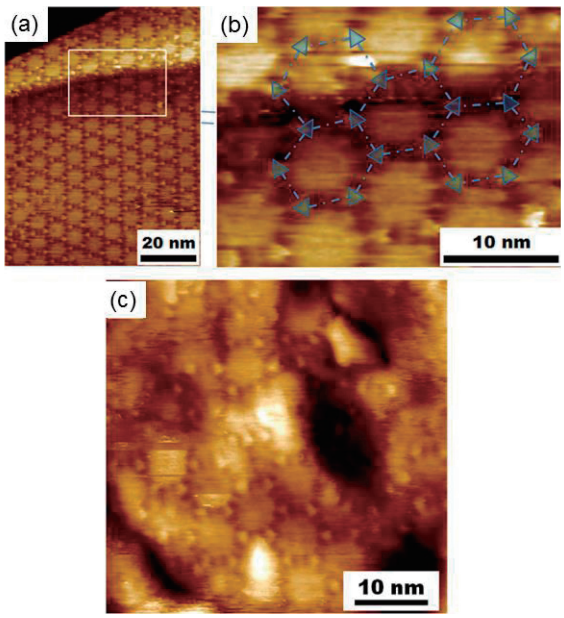

Figure 13. (a) Large-area STM image of the honeycomb pattern of **DBA-DAOC24OC25** at the TBC and epitaxial few-layer graphene grown on SiC. (b) Enlarged STM image of the areas marked by white square in (a). Blue triangles and dashed lines indicate the DBA cores and the alkyl chains, respectively. (c) STM image of the honeycomb pattern of **DBA-DAOC24OC25** at the TBC and CVD-grown single-layer graphene on polycrystalline Cu film on silicon wafer. Reprinted with permission from Ref. 44. Copyright 2013 American Chemical Society.

chains align parallel along the graphite main axes. We also observed significant effect of the substrate when Au(111) was used instead of HOPG; the most significant difference was the shapes of hexagonal structures of the porous network.[46,47]

Similar to the network patterns formed by DBAs at the TCB/graphite interface, both non-porous and porous patterns were observed at the TCB/Au(111) interface. The dominant patterns change depending on solute concentration and alkyl chain length as observed for the graphite interface. However, the most notable difference is the appearance of different polymorphs in the porous phases, which is due to positional difference for the van der Waals linkage between a pair of DBA molecules. Since there are two modes for alkyl group interdigitation, a supramolecular pair of DBAs becomes chiral depending on the interdigitation motifs, labeled arbitrarily (+) and (−) as shown in Figure 14a, in which the left DBA molecule locates with respect to the right one either above or below. The combination of six identical interdigitation motifs, either all (+) or all (−), produces a chiral hexagonal unit having inner alkyl chains directing either counterclockwise or clockwise direction as shown in Figure 14a. On the other hand, combination of two (+) and four (−) interdigitation modes leads a non-uniform hexagonal unit as depicted in Figure 14a bottom. Combination with different number of (+) and (−) modes will lead to further variation. Indeed, there are a total of eight possible hexagonal structures (12: if enantiomers are included) consisting of different interdigitation patterns as illustrated in Figure 14b.

We revealed that **DBA-OC6** formed a porous network consisting of chiral, achiral, and distorted hexagonal units, formed by uniform, alternating, and irregular alignments of DBA mole-

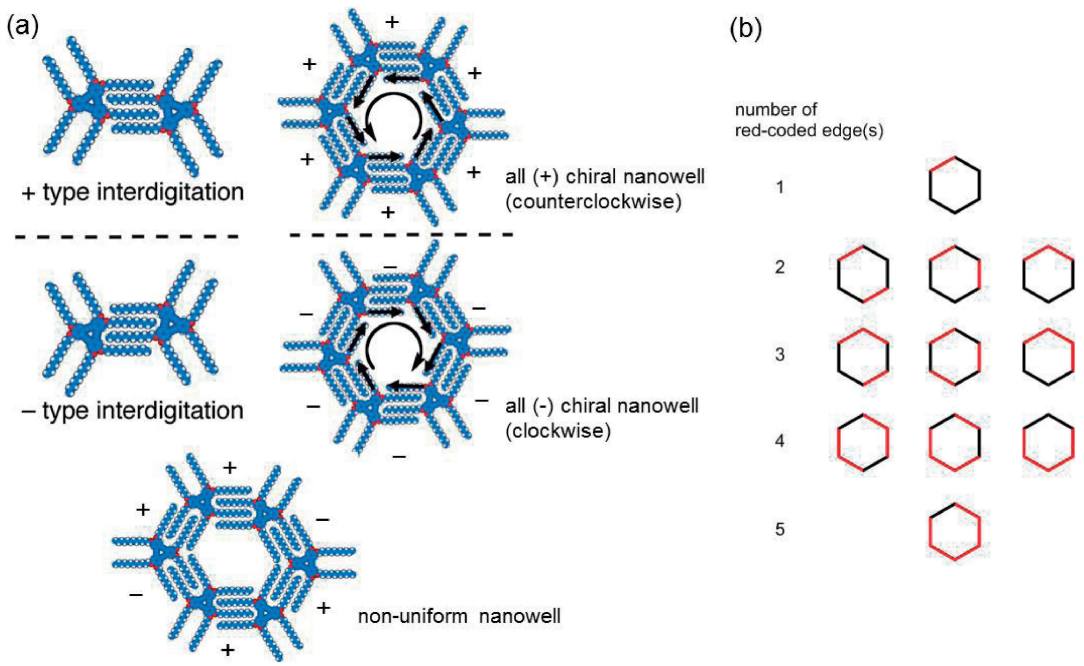

Figure 14. (a) Molecular models of (+) and (−) interdigitation patterns of **DBA-OC10** and a chiral hexagonal unit formed by all (+) type interdigitation pattern (top), all (−) type interdigitation pattern (middle), and a non-uniform hexamer formed by combination of (+) and (−) interdigitation motifs (bottom). The black arrows in the chiral nanowell indicate the counterclockwise and clockwise direction of the inner alkyl chains. (b) Models for all possible patterns of hexagonal units formed by combination of (+) and (−) interdigitation motifs are represented by red and black edge codes.

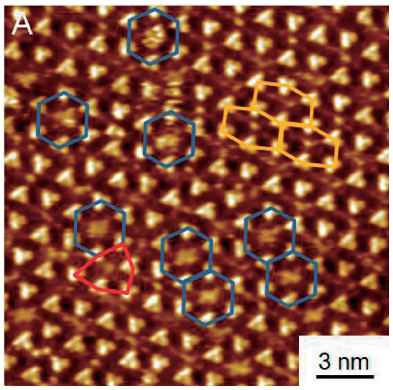

Figure 15. An STM image of a monolayer formed from **DBA-OC6** at the TCB/Au(111) interface at 1.3×10^{-4} mol L^{-1}. The blue, red, and yellow hexagons indicate chiral (uniform alignment), achiral (alternating alignment), and distorted (irregular alignment) nanowells, respectively. Reprinted with permission from Ref. 46. Copyright 2012 American Chemical Society.

cules, respectively, at the TCB/Au(111) interface (Figure 15).[46] Preliminary experiments showed this trend of forming irregular porous networks was also observed in DBAs with longer alkoxy chains. We tentatively attribute the formation of non-uniform hexagonal units at the TCB/Au(111) interface primarily to weaker alkyl chain–substrate interaction and mismatch of registry.

5. Adaptivity of Triangular Building Blocks in Self-Assembly at Liquid/Solid Interfaces

Since the fundamental criteria for the formation of porous molecular networks of DBAs was clarified as described in the previous chapter, we planned to modify the porous network for the purpose of using them as space to accommodate guest molecules in selective, active, and reversible manners with prospects of research that may find applications in tailor-made sensors and catalysts. It should be pointed out that the alkoxy chains in the DBA building blocks are not only physically modified by changing the alkyl chain length and its parity but also chemically functionalized by introduction of a stereogenic center or a functional group that would function as an active binding site in the nanowell.

Moreover, the substitution pattern on the DBA core can be controlled in such manners as an alternating substitution with different chains and functionalizing one among six alkyl chains. Based on this synthetic versatility of the DBA building blocks, we explored (i) pore size control by just changing the alkoxy chain length and size recognition for co-adsorption of aromatic guest molecules, (ii) study of the effect of even or odd number alkyl chains on the porous structure and the mixing behavior of DBAs bearing even/odd chains, (iii) generation, induction, and reversion of supramolecular chirality on surfaces by using DBAs bearing stereocenters in the alkoxy chains and, (iv) chemical modification of the pore interior for selective adsorption of guest molecules by introducing functional groups, which exert non-covalent interactions with the guest molecules or modify the pore size of the nanowell reversibly in response to external stimuli. In addition, we accidentally

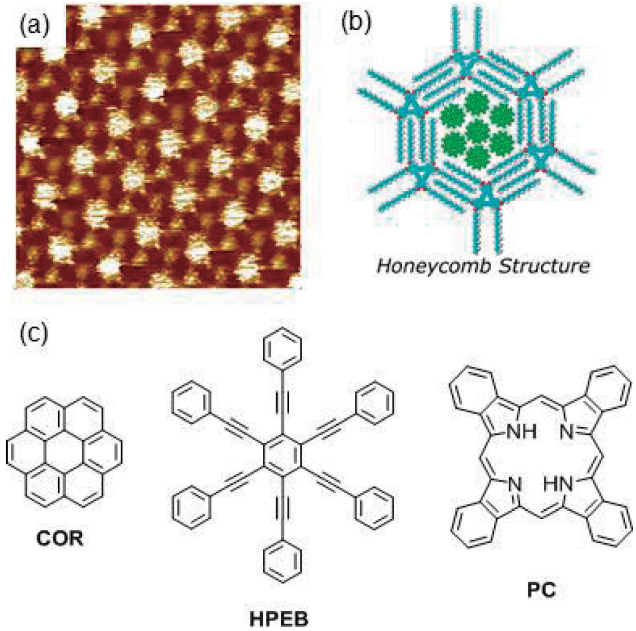

Figure 16. (a) STM image of the honeycomb network of **DBA-OC10** containing coronene (**COR**) molecules in the pores and (b) model of a honeycomb pore of **DBA-OC14** containing seven molecules of **COR**. (c) Chemical structures of hexakis(phenylethynyl)benzene (**HPEB**) and phthalocyanine (**PC**). Reprinted with permission from Ref. 48. Copyright 2007 John Wiley and Sons.

observed the formation of superlattice structures on surfaces that originate from steric interactions between DBAs with alkoxy chain of different parity, and co-adsorption of guest molecules.

5.1 Hexagonal Pore Size Control for Selective Guest Co-adsorption. As described in sections 4.3–4.4, by adjusting conditions we are able to form porous networks of DBAs consisting of hexagonal nanowells of diameters ranging ca. 1.6 nm (C6) to 4.7 nm (C20) at the liquid/solid interface. Solvent molecules are co-adsorbed to occupy the void space of the nanowells, and they are occasionally visualized by STM. However, when guest molecules which interact more strongly with the graphite surface than the solvent molecule are present, they can be immobilized in the nanowells by replacing the solvent molecules. The mode and ease of guest co-adsorption are dependent on the size- and shape-complementarity between the guests and nanowells. From this point of view, we investigated guest co-adsorption in the porous networks of DBAs and bisDBAs with respect to (i) structural transformation of the networks induced by co-adsorption of guest molecules, (ii) selectivity in immobilization of guest molecule clusters, and (iii) size- and shape-complementary in co-adsorption of two or three different guest molecules in the nanowells, forming multi-component 2D assemblies.

Our initial experiments on 2D host–guest chemistry were conducted using **DBA-OC10**–**DBA-OC16** at relatively high concentration (ca. 10^{-4} mol L^{-1} in TCB) and coronene (**COR**) as a guest molecule.[48] As shown in Figure 16a, in the honeycomb network of **DBA-OC10** bright but fuzzy spots are clearly visible which are assigned to co-adsorbed **COR** molecules,

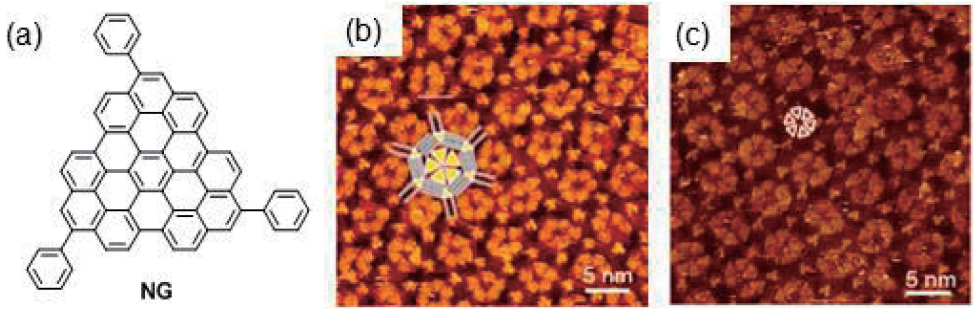

Figure 17. (a) Chemical structure of "nanographene" **NG**. STM images of (b) **DBA-OC18** containing mainly five **NG** molecules in the pores and (c) **DBA-OC20** containing mainly six **NG** molecules in the pores. Models are superimposed in (b) and white triangles in (c) indicate **NG** molecules. Reprinted with permission from Ref. 50. Copyright 2008 American Chemical Society.

though the exact number of the guests could not be determined. As described in section 4.3, at this concentration regime the non-porous patterns are the dominant network type of **DBA-OC14** and **DBA-OC16**. However, in the case of **DBA-OC14**, upon addition of excess **COR** to the non-porous pattern formed at the TCB/graphite interface, a nearly complete conversion into the honeycomb structure was observed. Though the exact number of **COR** guests could not be determined, a maximum of seven **COR** molecules can fit in the cavity as shown in the model (Figure 16b). However, this guest-induced structural transformation did not occur efficiently for **DBA-OC16**, although several honeycomb domains were observed. In addition to **COR**, hexakis(phenylethynyl)benzene (**HPEB**) and phthalocyanine (**PC**) also induced as guests the non-porous-to-porous transformation for **DBA-OC14** (Figure 16c), indicating the importance of adsorption energy of guest molecules to drive this structural change in spite of the different symmetry between the guest molecules and the host network.

The capacity of the hexagonal porous networks formed by DBAs to accommodate shape-compliment triangular guest molecules was examined. For this purpose, triphenyldiphenanthro-[3′,4′,5′,6′-*efghi*:3,4,5,6-*uvabc*]ovalene hereafter called "nanographene" **NG** (Figure 17a)[49] synthesized by Müllen was employed as a guest.[50] As expected, in the honeycomb network of **DBA-OC10** one molecule of **NG** was immobilized, though it was observed as a large fuzzy spot owing to the mobility. In the case of **DBA-OC12**, both fuzzy features due to mobile single **NG** and bright features with elongated rhombus-like shape which are ascribed to **NG** dimers were observed. The long axis of the dimers is always pointing to two opposite corners of the honeycomb pore, because the distance of the long axis of the dimer fits the corner-to-corner distance of the nanowell.

In the honeycomb network of **DBA-OC14**, no **NG** molecule was observed at submolecular resolution presumably due to its high mobility in the pore, and hence the number of **NG** molecules immobilized in the void could not be determined. Note, however, that the non-porous-to-porous transformation took place similarly to the case with **COR** guest. For DBAs with longer alkoxy chains, **DBA-OC16**, **DBA-OC18**, and **DBA-OC20**, honeycomb structures are formed nearly exclusively in the presence of **NG**, indicating stronger effect of **NG** than **COR** to induce structural transformation to the porous pattern due to stronger affinity to graphite. In these cases, the individual guest molecules could be identified clearly. For **DBA-OC16**, the number of guest molecules most frequently counted in each void was four, though it varied from 2 to 5. The orientation of the guest molecules is different from one pore to another, and the hexagonal shape of the nanowells is also deformed (see Figure 14). In the honeycomb network of **DBA-OC18**, five molecules of **NG** were observed most frequently (70%) as shown in Figure 17b. In the case of **DBA-OC20**, hexamers of **NG** are now the dominant species (85%) (Figure 17c). Because six molecules of **NG** occupy the size of the nanowell of **DBA-OC20** (4.7 nm from edge-to-edge), the **NG** hexamer looks like a sheet of pizza cut into six pieces. Thus the number of guest molecules embedded in each nanowell shows a clear dependence on the size of the pores. A few other examples for immobilization of guest clusters in the pores formed by molecular self-assembly are known.[5b,51]

Bimolecular clusters can also be immobilized in the hexagonal nanowells formed by DBAs. **COR** molecule serves as a guest for a cyclic assembly of six molecules of isophthalic acid (**ISA**) formed by hydrogen bonds between the carboxy groups. This supramolecular heterocluster is immobilized in the honeycomb network of **DBA-OC10** via van der Waals interaction, leading to a three-component 2D crystal.[52] Namely, at the OA/graphite interface, under which conditions **DBA-OC10** itself forms mainly the close-packed non-porous pattern, a mixture of **DBA-OC10**, **COR** and **ISA** revealed the structural transformation from non-porous to the nanoporous pattern. In each nanowell a heterocluster consisting of **COR** surrounded by six molecules of **ISA** is immobilized (Figure 18). For the higher homologue **DBA-OC12**, although its close-packed 2D network was also transformed into the honeycomb pattern upon addition of an excess of **COR+ISA**, the majority of the cavities appear fuzzy and featureless, possibly due to mobile **COR** molecules or **COR+ISA** cluster which does not fit to the nanowell. Only **DBA-OC10** immobilizes the **COR+ISA** clusters in its cavities, demonstrating the strict complementarity in size and shape for co-adsorption.

The hexagonal pores of the Kagomé network of **bisDBA-C12** can also be utilized to host the heterocluster of **COR+ISA**.[53] In addition, the smaller triangular space of the Kagomé network is filled with a complimentary guest, triphenylene (**TRI**), leading to the construction of a four-component 2D crystalline network. The experiments were also done using 1-octanoic acid as a solvent, under which conditions, **bisDBA-C12** formed exclusively a non-porous pattern. After fine-tuning for the molar ratio of the three guests (**COR**, **ISA**, and **TRI**) and **bisDBA-C12** to counterbalance a large difference in

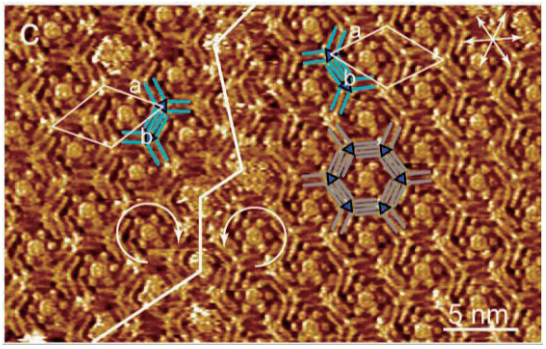

Figure 18. STM image of **DBA-OC10** containing in each nanowell a molecular cluster consisting of one **COR** surrounded by six **ISA** molecules. The white line and curved arrows indicate a domain boundary and CW/CCW chirality of the honeycomb structure in each domain. Models are superimposed. Reprinted with permission from Ref. 52. Copyright 2008 American Chemical Society.

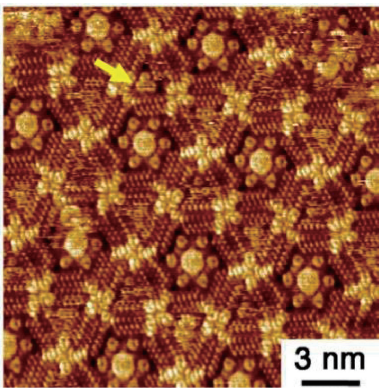

Figure 19. STM image of a mixture of **bisDBA-C12**, **COR**, **ISA**, and **TRI**. The yellow arrow points to a **TRI** molecule clearly visualized. Reprinted with permission from Ref. 53. Copyright 2009 John Wiley and Sons.

the molecule–substrate interactions, a Kagomé structure was formed (Figure 19). Each hexagonal void is filled with a **COR+ISA** cluster, whereas the triangular voids are filled by the **TRI** molecules. Control experiments showed that while only **COR+ISA** (without **TRI**) transformed the structure and the **COR+ISA** heteroclusters were immobilized in the hexagonal pores of the Kagomé structure, **COR** alone did not induce the structural transformation from the non-porous structure of **bisDBA-C12**. **TRI** also induced the formation of the Kagomé structure of **bisDBA-C12**, and it filled both the hexagonal and triangular pores. Modeling suggests that the size and shape of a cluster of six **TRI** molecules fits well to the hexagonal pore of **bisDBA-C12** like **NG** does for the nanowells of **DBA-OC20**. It seems therefore that both heterocluster **COR+ISA** and **TRI** are adsorbed to their best-fit positions when all three guests are mixed, indicating that the four-component 2D crystallization is a cooperative process involving a synchronized interplay of all components wherein the exact size matching between the guests (and guest clusters) to each pore space is crucial.

5.2 Odd-Even Effect. Odd-even effects in straight chain alkanes and alkyl groups are phenomena frequently observed in supramolecular chemistry. For example, it has been shown that

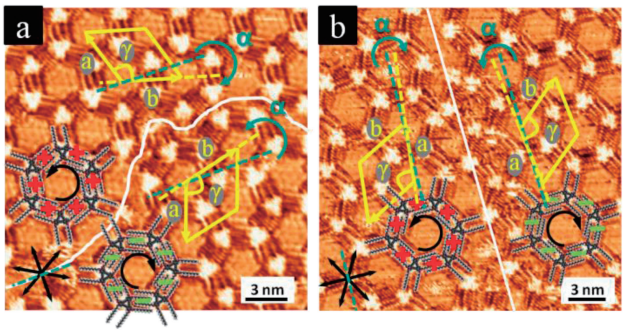

Figure 20. High-resolution STM images of mirror image domains of (a) **DBA-OC11** and (b) **DBA-OC12**. Unit cells are indicated in yellow. The HOPG main symmetry directions are represented by the black arrows at the left corner. The HOPG reference axis used to measure the angle α is highlighted by a turquoise dotted line and curved arrow. The CW and CCW domains have the alignment angles $+\alpha$ and $-\alpha$, respectively. The absolute values of α depend on even or odd number of the alkyl chains and the signs depend on chirality of the honeycomb domains. Reprinted with permission from Ref. 57. Copyright 2013 American Chemical Society.

in densely packed organic thin films of alkanes the molecules tend to exhibit an alteration of the network structures depending on the parity of the number of the methylene units.[54] Such effect is also observed in binary mixture systems; mixtures of primary linear alcohols that differ by one methylene group show ideal mixing if the shorter alcohol possesses an odd number of carbon atoms.[55] In contrast, if the shorter component is even, co-crystals are formed. The occurrence of mixing (random or ordered) on the surface rather than phase separation is ascribed to the similar symmetries of the unit cells of the pure components.[56] Similarly, odd-even effect was also observed in the self-assembled monolayers of DBAs in their single component systems as well as in binary mixtures of DBAs that differ by one methylene group as described below.[57] **DBA-OCn** derivatives with different alkyl chain lengths (n = 11–16) were used for the experiments on the odd-even effect at the 1-phenyloctane (PO)/HOPG interface.

In the simplified model described in Figure 14a, the alkoxy chains are drawn to orient orthogonal to the edge of the DBA cores. However, close inspections of the orientation of the monolayers with respect to that of the underlying graphite lattice reveal that the alkyl chain orientation is different between **DBA-OCn$_{odd}$** and **DBA-OCn$_{even}$** bearing alkoxy chains with odd or even number carbon atoms, respectively. Namely, the unit cell alignment angle α with respect to the HOPG lattice of the C_6-symmetric structures is different between **DBA-OCn$_{odd}$** and **DBA-OCn$_{even}$** as shown in Figure 20 for **DBA-OC11** and **DBA-OC12**. The mean angle α of the domains of **DBA-OCn$_{odd}$** (n = 11, 13, 15) is 13° whereas it is 4.5° for **DBA-OCn$_{even}$** (n = 12, 14, 16). The different angle α in the networks formed by **DBA-OCn$_{odd}$** and **DBA-OCn$_{even}$** was used as a diagnostic criterion to identify even or odd alkoxy DBAs in their binary mixtures as described below.

At the molecular level, the above tilt corresponds to the tilt of the alkoxy chains from the orthogonal orientation to the edge

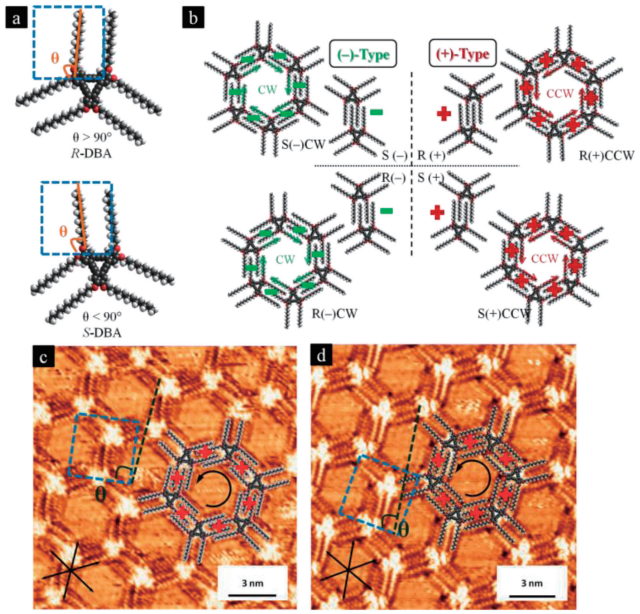

Figure 21. (a) Models showing molecular chirality of **DBA-OCn**, *R*-DBA ($\theta > 90°$) or *S*-DBA ($\theta < 90°$) generated by adsorption on a surface and (b) models for combination of the molecular *R*/*S* chirality of **DBA-OCn** to exhibit supramolecular chirality due to the alkyl chain interdigitation pattern yielding four different types of dimers and C_6-symmetric hexamers. (c) STM images of a CCW domain of **DBA-OC12** and (d) a CCW domain of **DBA-OC13**. The blue dotted square represents a 90° angle with respect to the edge of the DBA core, the dark dotted line indicates the alkyl chain direction, and the angle between them defines the tilt angle θ which is characteristic to **DBA-OC12** and **DBA-OC13**. The black curved arrow indicates the CW/CCW supramolecular chirality of the C_6-symmetric structure in each domain. Reprinted with permission from Ref. 57. Copyright 2013 American Chemical Society.

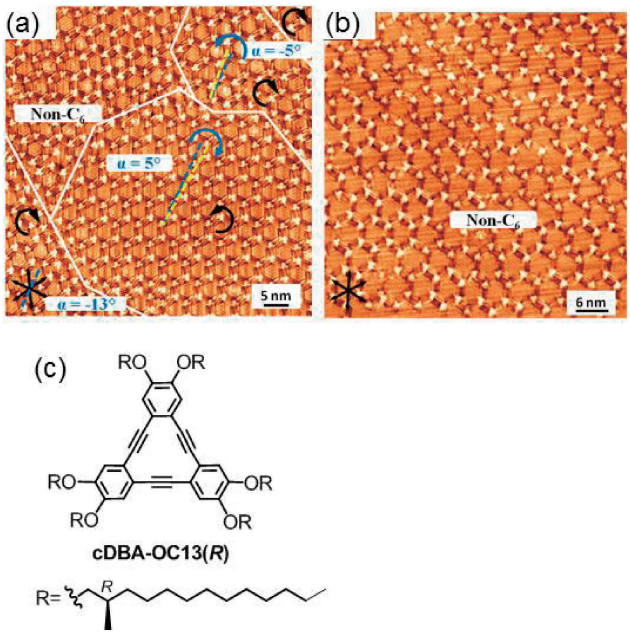

Figure 22. (a) STM image of **DBA-OC12**/**DBA-OC13** with domains of CW or CCW hexagons. The + (clockwise) or − (counterclockwise) direction of angle (α) between the unit cell vector (yellow dotted line) and the HOPG reference axis (blue dotted line) is indicated by blue curved arrow. The black curved arrow indicates the CW/CCW supramolecular chirality of the C_6-symmetric structure in each domain. The domain borders are highlighted by the white lines. (b) STM image of **DBA-OC15**/**DBA-OC16** in which the domain is covered with non-C_6-symmetric hexagons. (c) Chemical structure of **cDBA-OC13(*R*)**. Reprinted with permission from Ref. 57. Copyright 2013 American Chemical Society.

of the DBA cores. This means, in addition to supramolecular chirality arising from the (+)/(−) directions for the interdigitation of the alkyl chains on the surface (Figures 14a and 14b), each DBA molecule possesses also specific molecular chirality, here denoted as ***R*-DBA** or ***S*-DBA** depending on whether the angle denoted as θ of the alkyl chains with respect to the DBA edge is larger or smaller than 90° (Figure 21a). The experimentally measured values of angle θ for **DBA-OC12** are $85 \pm 3°$ or $95 \pm 3°$ (Figure 21c); the tilt angles of the alkyl chains from 90° are ca. 5°. The magnitude of the tilt angle from 90° for **DBA-OC13** is larger (Figure 21d), consistent with the larger magnitude of α than that of **DBA-OC12**. Therefore, at the level of DBA dimers four different combinations are possible (Figure 21b). While *R*(+)/*S*(−) and *R*(−)/*S*(+) pairs are enantiomeric and have the same stability, *R*(+)/*S*(+) or *R*(−)/*S*(−) are diastereomeric pairs and therefore should have different stability. Intriguingly, existence of a specific combination depends on the parity of carbons in the alkoxy chains: *R*(+) and *S*(−) for **DBA-OCn$_{even}$**, while *R*(−) and *S*(+) are most favorable for **DBA-OCn$_{odd}$** (Figures 21c and 21d). The observed odd-even effect in porous 2D assemblies originates from the asymmetry in van der Waals interactions of the interdigitated alkyl chains and DBA core, which was supported by molecular mechanics calculations for simplified dimer models.

An interesting odd-even effect was observed in bicomponent mixtures of **DBA-OCn** bearing alkoxy chains that differ by one methylene unit, including 1:1 (molar ratio) premixed solutions of **DBA-OC11**/**DBA-OC12**, **DBA-OC12**/**DBA-OC13**, **DBA-OC13**/**DBA-OC14**, **DBA-OC14**/**DBA-OC15**, and **DBA-OC15**/**DBA-OC16** in PO (total concentrations: ca. 10^{-6} mol L^{-1}). As shown in Figure 22 for mixtures of **DBA-OC12**/**DBA-OC13** and **DBA-OC15**/**DBA-OC16**, porous networks are formed for all mixtures. However, by detailed analysis of the relative abundance of different types of hexagonal pores, their distributions on the surface can be classified into two types; (A) when the alkoxy chains of **DBA-OCn$_{even}$** are smaller than that of **DBA-OCn$_{odd}$** (**DBA-OC12**/**DBA-OC13** and **DBA-OC14**/**DBA-OC15** systems), the surface is mainly covered with domains of porous patterns of C_6-symmetry (Figure 22a), and (B) when the alkoxy chains of **DBA-OCn$_{odd}$** are smaller than that of **DBA-OCn$_{even}$** (**DBA-OC11**/**DBA-OC12**, **DBA-OC13**/**DBA-OC14** and **DBA-OC15**/**DBA-OC16** systems), the surface is mainly covered with non-C_6-symmetric hexagons of lower symmetry (Figure 22b).

Though direct assignment of the adsorbed DBA molecules by STM is not possible because of the small difference

between the alkoxy chain lengths, for the regular hexagons of C_6-symmetry, it is possible to identify which DBA molecule constitutes each domain on the basis of the unit cell alignment angle α with respect to the HOPG lattice as described for single component networks (Figure 20). Namely, the angle α in the domains of C_6-symmetric hexagons formed from **DBA-OC12**/**DBA-OC13** and **DBA-OC14**/**DBA-OC15** mixtures show clear bimodal distribution with maxima at 5.1 and 12.9°, and 4.9 and 13.5°, respectively. The observed angles (ca. 5° and ca. 13°) correspond to those of the single component networks of **DBA-OCn$_{even}$** and **DBA-OCn$_{odd}$**, respectively. Consequently, it is deduced that self-assembly of the **DBA-OCn** mixtures in which n_{even} is smaller than n_{odd} leads to phase separation on the surface (Figure 22a).

For the disordered phase formed by **DBA-OCn** mixtures in which n_{odd} is smaller than n_{even}, similar analysis cannot be applied, because disorder indicates random mixing of both components. To confirm the random mixing, we used as a marker molecule **cDBA-OC13(*R*)** (Figure 22c) which has a stereocenter in each alkoxy chain, because it can be readily distinguished from DBAs without stereocenters by its appearance with dark edges as described in the next section. As expected, a binary mixture of **DBA-OC12** with **cDBA-OC13(*R*)** exhibited phase separation, wherein domains consisting of hexagons with dark contours (domains of **cDBA-OC13(*R*)**) and those without the marker (domains of **DBA-OC12**) were observed. In contrast, for a solution of **cDBA-OC13(*R*)**/**DBA-OC14**, dark contour molecules are distributed randomly, confirming random mixing of two components in the disordered domains.

While thermal annealing of mono-component systems leads to disappearance of the lower symmetry hexagons, leading to larger domains of the ordered hexagonal networks, unexpectedly, annealing of the disordered domains formed by a mixture of **DBA-OC11** and **DBA-OC12** led to a formation of a superlattice structure comprising both C_6- and C_2-symmetric pores as described below. The formation of such complex self-assembled systems of high level of periodicity, typically called superlattice or superstructure, remains a challenge in on-surface 2D supramolecular chemistry, in spite of intense interest in understanding principles governing highly organized architectures and potential applications in nanopatterning.[58]

Similar to the mono-component systems, annealing DBA mixtures in which **DBA-OCn$_{odd}$** was larger than **DBA-OCn$_{even}$** resulted in disappearance of all non-C_6-symmetric pores, which co-existed at room temperature, leaving on the surface only large separated phases of pure components. Interestingly, although the experiments were done with equimolar mixtures of DBAs, at elevated temperatures there was significant preferential adsorption (>90%) of shorter DBAs with even-numbered alkyl chains because of larger adsorption energy of **DBA-OCn$_{even}$** due to better matching in alkyl chain interdigitation. On the other hand, thermal annealing of DBA mixtures in which **DBA-OCn$_{even}$** was larger than **DBA-OCn$_{odd}$** led to the formation of a new highly ordered structure comprising both C_6- and C_2-symmetric pores (Figures 23a–23d). This structure has two distinct sites; DBAs forming C_6-symmetric rings and single DBAs connecting those rings into the perfectly hexagonal superstructure by forming six surrounding C_2-symmetric rings (Figure 23e). Such superstructure was never observed in self-assembly of single component systems and thus has to contain both components. Finally, experiments with marker molecules (**cDBA-OC13(*R*)+DBA-OC14** mixture) have allowed to identify that in the superstructure **DBA-OCn$_{even}$** and **DBA-OCn$_{odd}$** occupy the C_6-symmetric and C_2-symmetric sites, respectively.

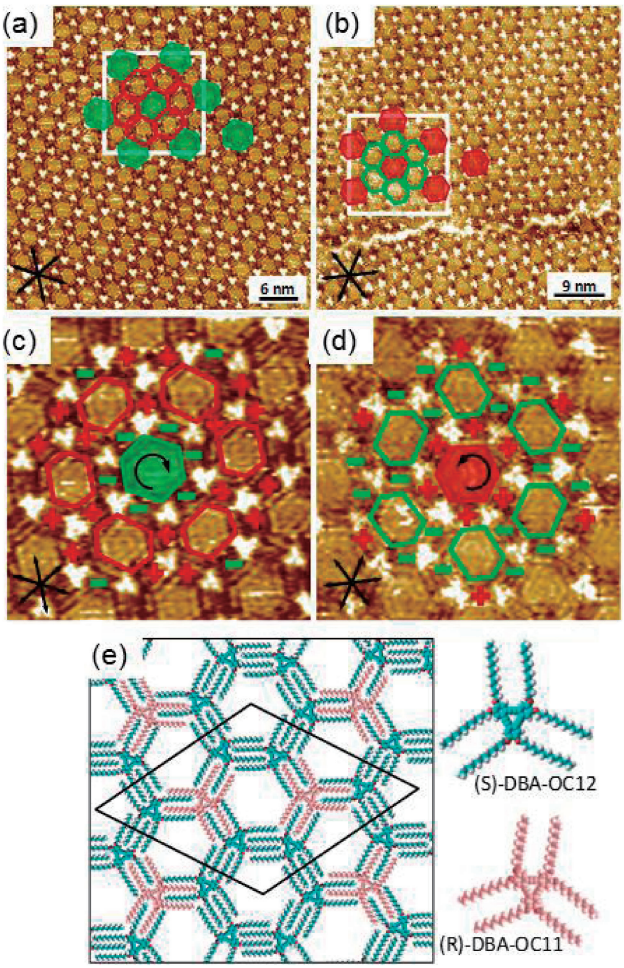

Figure 23. (a, b) STM images of the 1:1 binary mixture of **DBA-OC11**/**DBA-OC12** after a thermal annealing at 80 °C. New chiral superstructure is observed containing ordered combinations of chiral C_6- (filled green or red) and achiral C_2-symmetric (open green or red) hexagons. (c, d) Enlarged areas inside the white squares of the corresponding top images. (e) A molecular model of the supramolecular structure of the highly ordered 2D co-assembly formed from **DBA-OC11** and **DBA-OC12** after thermal annealing. Reprinted with permission from Ref. 57. Copyright 2013 American Chemical Society.

Molecular mechanics calculations support the different behavior depending on the parity of the larger/smaller alkyl chains of the DBA mixtures. When n_{odd} is larger than n_{even}, the energy of intermolecular interactions of the heterodimer is lower than the average of intermolecular binding energies of the homodimers, due to a mismatched interdigitation of the alkyl chains and ineffective packing with a gap between some of the methyl groups of **DBA-OCn$_{even}$** and DBA cores of **DBA-OCn$_{odd}$**. In this case phase separation is favored as observed

experimentally. On the other hand, when n_{even} is larger than n_{odd}, the energy of intermolecular interactions of the heterodimer is higher than the average of intermolecular binding energies of the homodimers due to matched interdigitation of the alkyl chains, leading to a favorable mixing of both DBAs.

In the bi-component systems of **DBA-OCn$_{even}$** bearing alkyl chains that differ by more than two methylene units, phase separation or mixing behavior was observed depending on the mixed components. For binary mixtures which differ in the alkoxy chain length by two methylene units, mixed domains are observed in addition to phase-separated domains of each component. For example, a mixture of **DBA-OC14** and **DBA-OC16** exhibits phase separation with pure domains of the porous pattern of **DBA-OC14** and the nonporous pattern of **DBAOC16** and a considerable fraction of mixed domains consisting of both components at the TCB/graphite interface.[59] However, for a mixture of larger alkoxy DBAs such as **DBA-OC16** and **DBA-OC18**, it becomes difficult to evaluate the phase behavior because of the smaller proportional difference between the alkoxy chain lengths. As the alkoxy chain length difference increases to four methylene units, such as **DBA-OC14** and **DBA-OC18**, the phase separation becomes more pronounced, due to the increased difference in their unit cell parameters. For mixtures **DBA-OC14**/**DBA-OC20** and **DBA-OC10**/**DBA-OC20** with larger alkoxy chain length differences, complete phase separation was observed without mixing.

On the basis of the above observations, we predicted that a DBA molecule containing four short and two long alkyl chains would self-assemble to form porous networks by recognizing the alkyl chain of equal lengths. Therefore we designed a C_{2v} building block, **DBA-(OC10)$_2$OC20**, with four C10 and two C20 alkyl chains (Figure 24). We expect the formation of two different porous networks belonging to plane groups of *p*2 and *p*6.[7a] We indeed found that under certain conditions with regard to solvent, concentration, and temperature, either *p*2 or *p*6 pattern can be exclusively formed at the solvent/HOPG interface despite the fact that they have nearly equal packing densities.[60]

At low concentration in TCB (4.5×10^{-6} mol L^{-1}) **DBA-(OC10)$_2$OC20** formed a porous monolayer consisting of the *p*2 and *p*6 structures in an approximate ratio of 7:3 at room temperature (Figure 25). However, annealing at 50 °C resulted in the transformation into the *p*2 form exclusively, indicating it is a thermodynamically more favorable phase. This is in accord with the Monte Caro simulations of a simplified model on a surface, which indicate that the *p*6 structure is metastable with exceptionally long lifetime. On the other hand, whereas the *p*2 and *p*6 domains were observed in a nearly 1:1 ratio in PO at 3×10^{-6} mol L^{-1}, at very dilute conditions (1×10^{-6} mol L^{-1}) the *p*6 structure was observed exclusively. The preference of the *p*6 form in PO may be due to favorable co-adsorption of the solvent molecules in the pores, stabilizing this form. The resulting nanowells were utilized for selective adsorption of guest molecules and their clusters through precise recognition of the size and shape of the porous space.

5.3 Supramolecular Chirality. Prochiral molecules in three-dimensional (3D) space can become chiral when confined at a surface, as exemplified by 1-nitronaphthalene and naphtho-

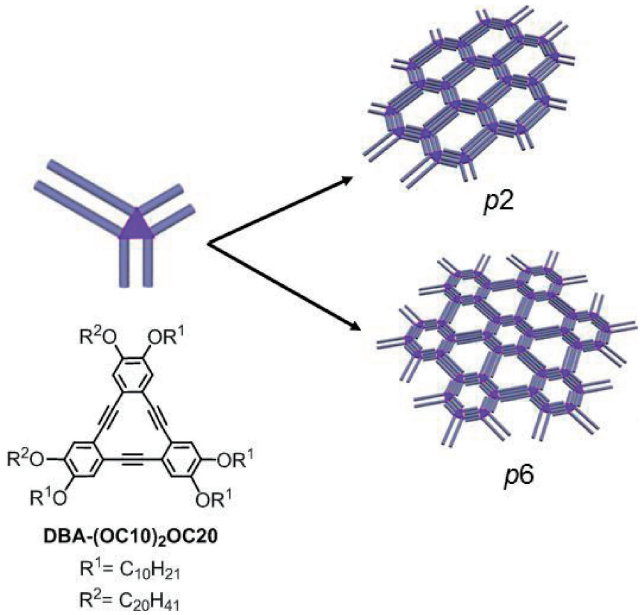

Figure 24. Schematic representation for the formation of two porous networks of *p*2 and *p*6 types by self-assembly of C_{2v} building block, **DBA-(OC10)$_2$OC20**. Reprinted with permission from Ref. 60. Copyright 2012 American Chemical Society.

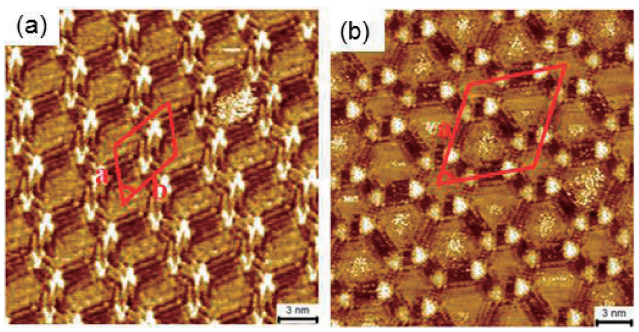

Figure 25. STM images of (a) the *p*2 symmetry packing and (b) *p*6 symmetry packing of the self-assembled monolayer of **DBA-(OC10)$_2$OC20** at the TCB/HOPG interface. Reprinted with permission from Ref. 60. Copyright 2012 American Chemical Society.

[2,3-*a*]pyrene which form chiral domains by adsorption.[61,62] These chiral domains are formed in equal proportions in the absence of any chiral bias, maintaining the system globally achiral. On the other hand, molecules which do not exhibit chirality at a single molecular level can assemble on a surface to produce homochiral domains exhibiting supramolecular chirality.[63] Moreover, addition of a small amount of a chiral molecule to a self-assembled monolayer of achiral molecules can perturb the distribution of left- and right-handed domains, ultimately to either one of handedness.[64] This is a 2D analog of the *sergeant-and-soldier* principle, that has been extensively studied for control of supramolecular chirality in 3D space.[65]

As described above in Figures 14 and 21, this is also the case for DBAs bearing simple alkoxy chains; although they are achiral in 3D space, they exhibit chirality at not only molec-

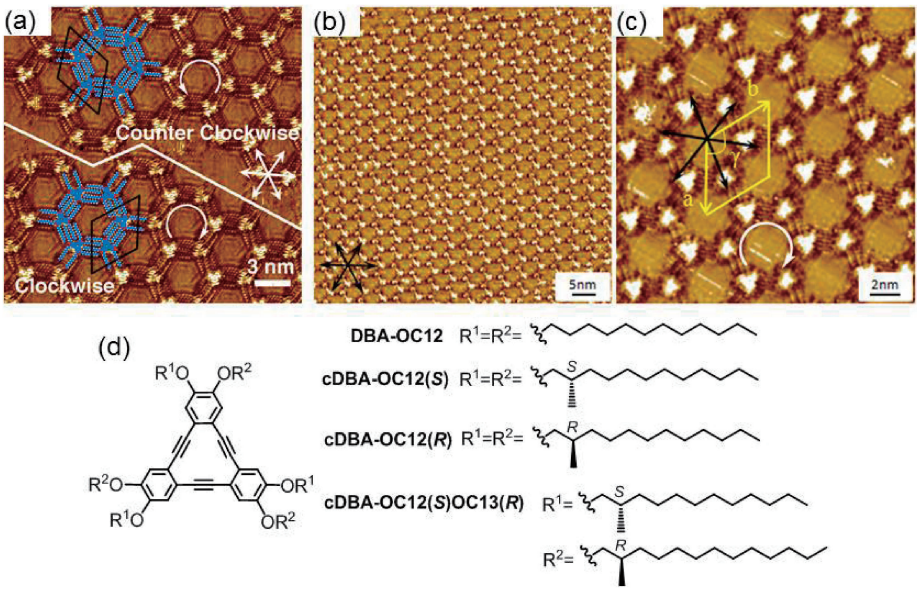

Figure 26. (a) STM image showing CW and CCW domains of **DBA-OC12** with domain boundary between them indicated by the white line. (b, c) STM images of **cDBA-OC12(*S*)** in which the domain is covered by the CW pattern. (d) Chemical structure of **DBA-OC12**, **cDBA-OC12(*S*)**, **cDBA-OC12(*R*)**, and **cDBA-OC12(*S*)OC13(*R*)**. Reprinted with permission from Ref. 66. Copyright 2011 Macmillan Publishers Limited.

ular but also supramolecular levels in 2D. For example, **DBA-OC12** forms enantiomeric domains, i.e., clockwise (CW) and counterclockwise (CCW) domains each consisting of (−) and (+) interdigitation patterns of the alkyl chains, respectively (Figure 14), in equal proportions. Figure 26a shows CW and CCW domains of **DBA-OC12** at the PO/graphite interface with a domain boundary between them. By using chiral DBAs (cDBAs) bearing a chiral center at C2-position of each alkyl chain instead of achiral **DBA-OC12**, we were able to control the global chirality. In addition, chirality induction was achieved for self-assembled monolayer of **DBA-OC12** by addition of the chiral DBA as a chiral inducer via a sergeant-and-soldier mechanism. Moreover, we incidentally found another, unique chirality induction mechanism, which was different from the sergeant-and-soldier mechanism, resulting in the reversal of chirality of monolayer of **DBA-OC12**.[66]

By simply using chiral **cDBA-OC12(*S*)** (Figure 26d) having *S* stereochemistry at the chiral center in each alkyl chain, the surface was covered entirely by CW domains at the PO/HOPG interface (Figures 26b and 26c). Use of the enantiomer **cDBA-OC12(*R*)** or its homologue **cDBA-OC13(*R*)** (chemical structure: Figure 22c) resulted in the formation of homochiral, antipodal CCW monolayer.[66] This observation can be explained in terms of steric effect of the stereogenic methyl groups in the interdigitated alkyl chain of two neighboring DBA molecules. For example, when **cDBA-OC12(*S*)** molecules are linked by alkyl chain interdigitation, three methyl groups in a molecule orient "up" with respect to the graphite surface, whereas the other three are imposed to orient "down" because the alkyl chains adopt a nearly straight, extended conformation (Figure 27a) The latter three methyl groups are located intrinsically under an unfavorable environment due to steric repulsion to the graphite surface. When two adjacent alkyl chains in a **cDBA-OC12(*S*)** molecule are interdigitated with a counterpart molecule, there are two possible interdigitation patterns, (−) and (+), similar to the case of achiral DBAs. However, their steric environments are different; in the (−) mode, the up-oriented methyl groups locate at the inner position, whereas the down-oriented methyl groups are at the outer position. The situation is reversed in the (+) mode, wherein the up- and down-oriented methyl groups locate at the outer and inner positions, respectively. The latter (+) mode is less favorable than the (−) mode, because it will be more difficult to avoid steric repulsion for the down-oriented methyl groups when they locate at inner rather than outer positions. Molecular mechanics calculations done for model hexamers composed by six **cDBA-OC12(*S*)** (two alkoxy chains in a molecule replaced by methoxy groups) arranged in (−) and (+) modes on a bilayered graphene supported this view; the model hexamer of the (−) mode is 9.7 kcal mol^{-1} more stable than that of the (+) mode (Figures 27b–27e).

cDBA-OC12(*S*) served as a chirality inducer for the self-assembled monolayer of achiral **DBA-OC12**. **cDBA-OC12(*S*)** was premixed in PO solution of **DBA-OC12** at different ratios, biasing the 2D chirality toward the CW form (Figure 28a).[66,67] However, chirality induction was not very efficient; a homochiral CW system was achieved by mixing **cDBA-OC12(*S*)** by up to 30%. To improve the efficiency of chirality induction **cDBA-OC12(*S*)OC13(*R*)** (chemical structure: Figure 26d), having C12 alkyl chain with an *S* stereocenter and C13 alkyl chain with an *R* stereocenter in an alternate fashion, was derived from **DBA-OTBS/OMOM** bearing orthogonal protecting groups. **DBA-OTBS/OMOM** in turn was prepared selectively by cross-coupling reaction of iodoalkyne **2**, which was readily derived from commercially available dimethoxybenzaldehyde **1** (Scheme 1). It should be pointed out that due to the *S*,*R* stereochemistry at the stereocenters, all methyl groups of **DBA-OC12(*S*)OC13(*R*)** can orient "up" with respect

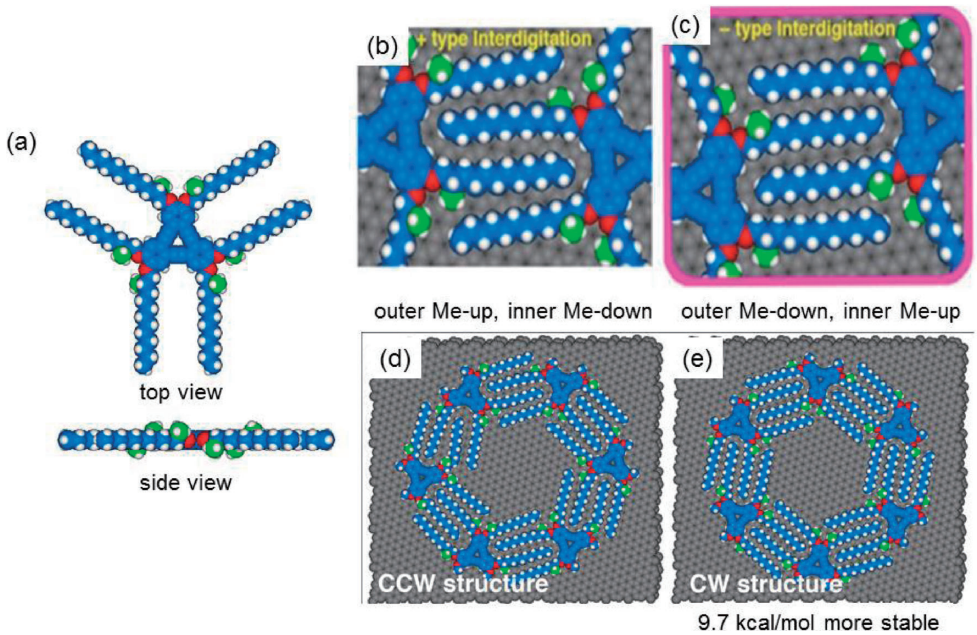

Figure 27. (a) Top and side views of a molecular model of **cDBA-OC12(*S*)**. Methyl carbon atoms are shown in green. (b, c) (+) and (−) interdigitation modes of alkyl chains, respectively, of a pair of **cDBA-OC12(*S*)** molecules. (d, e) Model hexamers of **cDBA-OC12(*S*)** having CCW and CW structures, respectively, assembled on a bilayered graphene. Reprinted with permission from Ref. 66. Copyright 2011 Macmillan Publishers Limited.

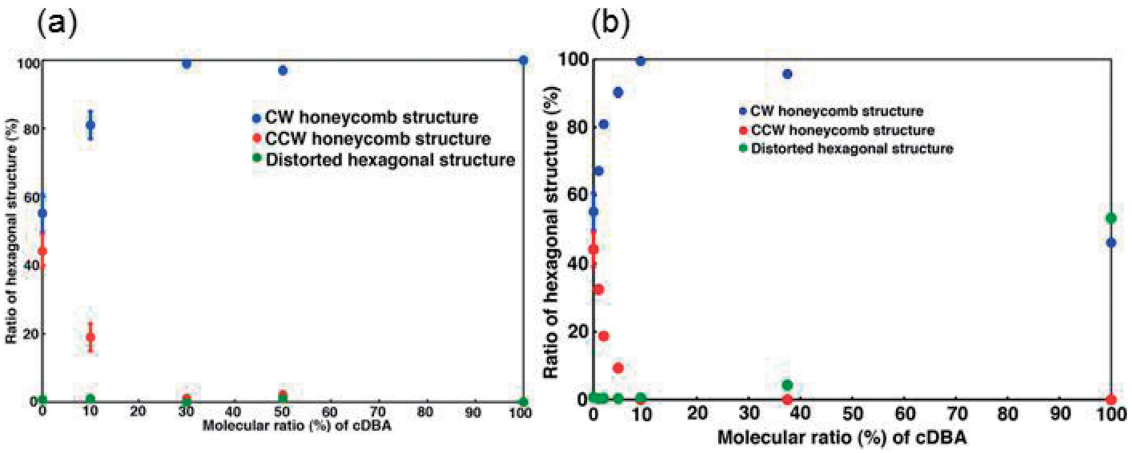

Figure 28. (a) Composition-dependent induction of 2D chirality of the self-assembled monolayer of **DBA-OC12** by **cDBA-OC12(*S*)**, showing the ratio of the CW (blue) and CCW (red) structures as well as distorted hexagonal structure (green). (b) The result of the same experiments using **cDBA-OC12(*S*)OC13(*R*)** as an inducer. Reprinted with permission from Ref. 66. Copyright 2011 Macmillan Publishers Limited.

to the graphite surface, in contrast to the case of **DBA-OC12(*S*)** (Figure 27a). Due to the additional steric effect arising from the match/mismatch between the alkyl chain lengths (C12 vs. C13) of **cDBA-OC12(*S*)OC13(*R*)** and **DBA-OC12**, the efficiency of chirality induction was improved considerably; by mixing 10% of **cDBA-OC12(*S*)OC13(*R*)** the entire system turned to the CW structure (Figure 28b).

In the STM images containing cDBAs, we found some of the DBA cores look as if they have black edges around the bright triangles (Figure 29a). Although we do not understand the exact reason for the different appearance, we attribute such DBA core to those of cDBAs, because they were observed only when cDBA was mixed. The proportion of the black-edge DBA was essentially identical to that of cDBA in solution when **cDBA-OC12(*S*)OC13(*R*)** was mixed as a chirality inducer, indicating similar adsorption energies of **cDBA-OC12(*S*)-OC13(*R*)** and **DBA-OC12**. On the other hand, the ratio of the black-edge DBA was much less when **cDBA-OC12(*S*)** was used, implying smaller adsorption energy of **cDBA-OC12(*S*)** than that of **DBA-OC12**. This is consistent with the fact that while **cDBA-OC12(*S*)OC13(*R*)** does not have "down" methyl groups due to its *S*,*R* configurations of the stereo centers, **cDBA-OC12(*S*)** has three unfavorable methyl groups as discussed above (Figure 27a).

During the course of our research on 2D chirality, we encountered unexpectedly several interesting observations. First, we noticed an interesting phenomenon, which we refer to as enantioselective quasi-self-adsorption.[68] As described above, a

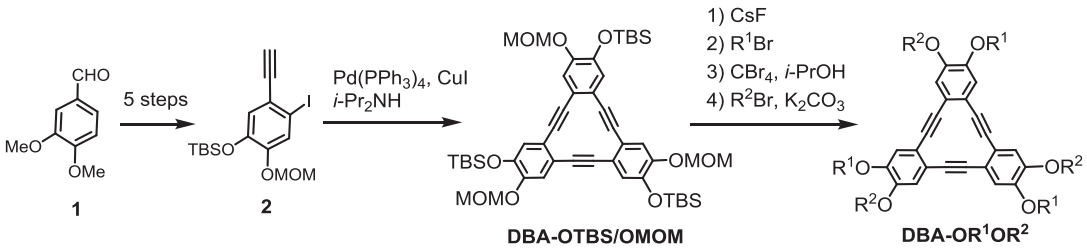

Scheme 1. Key steps for preparation of alternately substituted DBA, **DBA-OR^{1}OR^2**, including **cDBA-OC12(*S*)OC13(*R*)** from **DBA-OTBS/OMOM**, which was prepared from dimethoxybenzaldehyde **1** via iodoalkyne **2**.

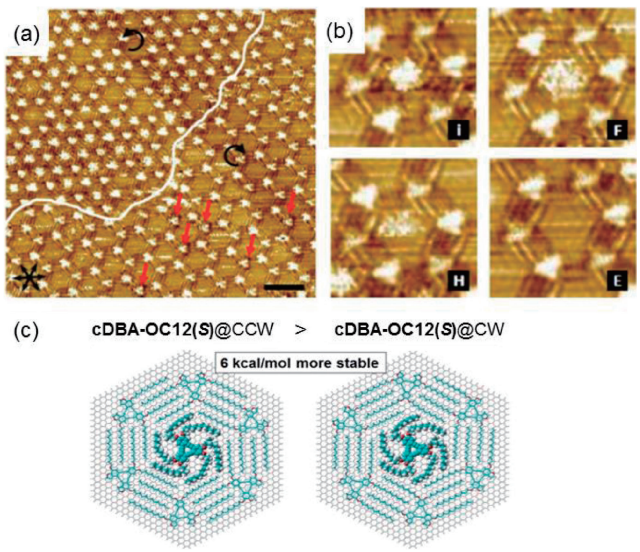

Figure 29. (a) STM image of a premixed solution containing 30 mol % **cDBA-OC12(*S*)** and 70 mol % **DBA-OC12**. The white line marks the boundary between a CCW domain (upper left) and CW domain (lower right). The scale bar measures 5 nm. The red arrows indicate **cDBA-OC12(*S*)** molecules with black rims incorporated in the network of **DBA-OC12**. (b) Examples of different types of pores: clear, fuzzy, half and empty observed using 30 mol % **cDBA-OC12(*R*)** and 70 mol % **DBA-OC12**. In the clear image the alkyl chains of the gust molecules are marked with red arrows. (c) Model hexamers of CCW form (left) and CW form (right) of **DBA-OC12** on a frozen graphene flake bearing **cDBA-OC12(*S*)** in the nanowell. Reproduced from Ref. 68 with permission from The Royal Society of Chemistry.

premixed solution of 30 mol % **cDBA-OC12(*S*)** and 70 mol % **DBA-OC12** at a total concentration of 2.5×10^{-6} mol L^{-1} self-assembles at the PO/graphite interface, forming amplified clockwise (CW) hexagons (95 ± 3% CW structure). As shown in Figure 29a lower right, in the CW network **cDBA-OC12(*S*)** molecules are identified due to the dark rim around the bright central triangular core, indicating they serve as chirality inducers via the sergeant-and-soldier mechanism.

While most of the pores in the network are empty, some pores appear brighter than the rest, imaged in different appearance (assigned as incorporated (I), fuzzy (F), and half-fuzzy (H) shown in Figure 29b), suggesting that such pores are filled by molecular species. The different occupation appearance of the guest must be due to their different mobility. Interestingly, there is a clear difference in occupation of the pores of CW and CCW domains; assuming that the nanowells are occupied for all three types of guest appearance, the CCW domains shows a higher degree of occupied pores than the CW domains; only 34% CCW pores are empty in contrast to 85% empty pores in the CW domains. The opposite tendency was observed for monolayers formed from mixtures of **cDBA-OC12(*R*)** and achiral **DBA-OC12**; only 63% CW pores are empty versus 83% CCW empty pores.

We attributed the species entrapped in the nanowell to cDBA molecules, because the guest was preferentially adsorbed in CCW domain when **cDBA-OC12(*S*)** was used as an inducer, and the mirror image relationship was observed depending on whether **cDBA-OC12(*S*)** or **cDBA-OC12(*R*)** was used. Moreover, for the bright feature assigned as incorporated, the guest molecules appear as a bright round blob surrounded with some kind of fine structure. The bright blob and the surrounding fine structure are tentatively attributed to the cDBA core and alkyl chains, respectively (Figure 29b (I)), suggesting cDBA molecule is incorporated in the nanowells in its windmill-like conformation. To confirm the preferential adsorption in the CW or CCW nanowells, molecular mechanics calculations were performed for CW and CCW type **DBA-OC12** hexamer models incorporating **cDBA-OC12(*S*)** in its windmill-like shape (Figure 29c). As a result, **cDBA-OC12(*S*)** in the CCW nanowell is more favourable than in the CW form by 6 kcal mol^{-1}. The major contribution to this energy difference is less van der Waals contacts between the methylene units when the chirality of the host does not match the direction of the windmill-like conformation of the guest. Thus it appears that chiral recognition occurs via alkyl chain interactions.

In the above quasi-self-adsorption, only cDBA serves as a guest, whereas more abundant achiral DBA does not. The reason for this selectivity can be explained in terms of the unfavorable methyl groups in cDBA as shown in Figure 30. Namely, for cDBA with the same sense of chirality in a molecule such as **cDBA-OC12(*S*)** or **cDBA-OC12(*R*)**, three methyl groups must orient "down" when the alkyl chains adopt a straight conformation as described above (Figure 27a). Even when excess cDBA molecules to serve as chirality inducers are present in solution as in the present case, they cannot be adsorbed as far as the alkyl chains maintain the straight conformation due to smaller adsorption energy compared to achiral DBA. On the other hand, if the alkyl chains bearing the unfavorable methyl groups turn to adopt a bent conformation, the methyl groups orient "up," avoiding the unfavorable interaction and thereby

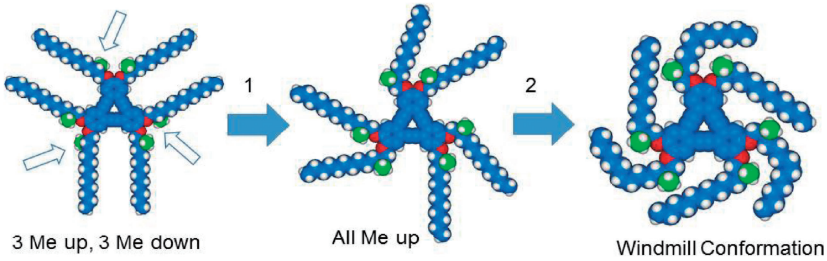

Figure 30. Schematic presentation for the conversion from straight alkyl chain to windmill conformations of **cDBA-OC12(*S*)**. Methyl carbon atoms are shown in green. (Step 1) The unfavorable methyl groups indicated by open arrows turn to orient the methyl groups "up" thereby making the alkyl chain bent. (Step 2) Bending of the other three alkyl chains in the same direction forming the windmill-like shape.

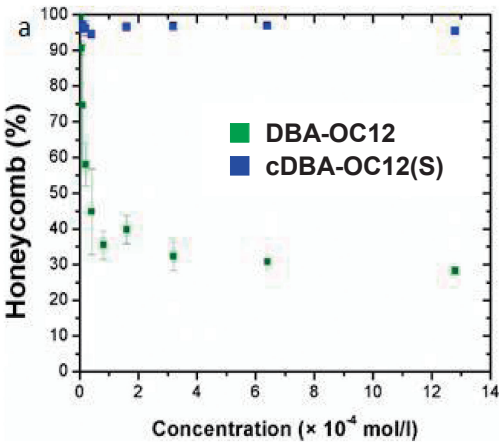

Figure 31. Dependence of honeycomb coverage of **DBA-OC12** (green squares) and **cDBA-OC12(*S*)** (blue squares) on the concentration of PO. Reprinted with permission from Ref. 69. Copyright 2015 AIP Publishing LLC.

making adsorption energy larger. Bending the remaining three alkyl chains in the same direction results in the windmill-like shape in a homochiral direction. In this form cDBA molecule is competitive enough to be adsorbed in the nanowells which is otherwise occupied by mobile solvent molecules.

The second unexpected observation is the selectivity between linear vs. honeycomb patterns.[69] It was revealed that **cDBA-OC12(*S*)** showed remarkably higher preference to form honeycomb network compared to achiral **DBA-OC12**. As described in sections 4.3, solute concentration affects significantly the selectivity toward the formation of densely packed linear or porous honeycomb networks of simple DBAs at the TCB/graphite interface; at low concentration the porous network is promoted, while at higher concentration the densely packed linear structure is favored. Concentration dependence of **cDBA-OC12(*S*)** was investigated at the PO/HOPG interface and compared with **DBA-OC12** in the concentration range of 2.5×10^{-6} to 1.3×10^{-3} mol L^{-1}.

As shown in Figure 31, where the honeycomb coverage is plotted as a function of concentration, the honeycomb structure of **cDBA-OC12(*S*)** turned out to be much less sensitive to the concentration compared to achiral **DBA-OC12**. The composition of the honeycomb structure of **cDBA-OC12(*S*)** is almost independent on the concentration; even at such high concentration as 1.3×10^{-3} mol L^{-1}, the honeycomb structure still occupies more than 90% of the surface area. In contrast, in the case of **DBA-OC12**, the concentration should be lower than 1×10^{-5} mol L^{-1} to maintain the porous network with the coverage of more than 90%.

In order to understand these differences in honeycomb coverage between chiral and achiral DBAs, the thermodynamic model of eq 1 (section 4.3) was applied. The experimentally obtained K value for **cDBA-OC12(*S*)**, which represents an equilibrium constant for the transition from a linear phase into a porous phase (see Figure 9), has a larger share of porous phase ($K = 26.3$) compared to **DBA-OC12** ($K = 0.14$), consistent with the STM observation. The slope m of eq 1 represents the ratio of molecular density between the porous and linear phase in a particular system. For **cDBA-OC12(*S*)**, the experimentally determined m value from the unit cell parameters was 1.01, implying an equal packing density of the porous and linear phase, which is counterintuitive in view of the clearly different unit cells. However, as can be seen in one of the nanowells in Figure 26c, fuzzy features attributed to mobile **cDBA-OC12(*S*)** molecules trapped inside were observed. The presence of additional **cDBA-OC12(*S*)** molecules inside the honeycomb nanowells results in a larger packing density, explaining the smaller m value than that expected from the unit cell parameters. Thus **cDBA-OC12(*S*)** exhibits higher preference to form the honeycomb network compared to achiral **DBA-OC12** at the PO/graphite interface due to true self-adsorption in its nanowell to stabilize the honeycomb phase by increasing the surface density. The smaller m value of 1.23 for **DBA-OC12** than that in TCB (1.53) can also be explained in terms of self-adsorption of **DBA-OC12** in its nanowell in PO solution, which is negligible in TCB.

The third unexpected observation was a most impressive phenomenon, chirality reversal.[70] During the experiments using chiral DBAs thus far described, we did not pay special attention to the effect of solute concentration and temperature on 2D chirality. However, as we revealed an important role of temperature in determining the linear vs. porous networks of achiral DBAs (section 4.4), we found crucial effects of solute concentration and temperature on chirality induction mechanisms of the molecular networks.

A low-concentration solution of **DBA-OC12** in PO containing 10 mol % **cDBA-OC12(*S*)** (5.0×10^{-7} mol L^{-1}) on HOPG exhibited 91% CW structure at room temperature. When this solution was annealed slowly (2 °C min^{-1}) to 80 °C (STM observation done after cooling down to room temperature),

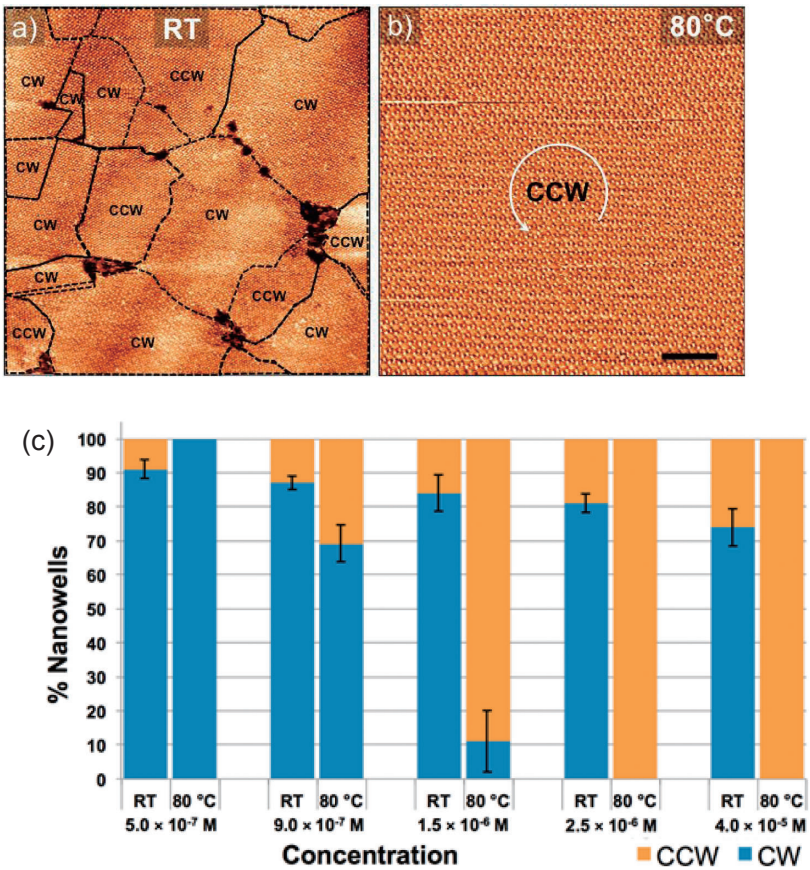

Figure 32. (a) STM image of **DBA-OC12** containing 10 mol % **cDBA-OC12(*S*)** at the PO (2.5×10^{-6} M)/HOPG interface at room temperature. The surface consists of 81% CW and 19% CCW nanowells. (b) STM image of the same solution after annealing at 80 °C followed by cooling down to room temperature. The surface is covered entirely by the CCW domain. (c) Histograms of concentration-dependent chirality induction observed at room temperature and after annealing at 80 °C. The orange and blue bars indicate CCW and CW domains, respectively. Reprinted with permission from Ref. 70. Copyright 2016 Macmillan Publishers Limited.

coalescence of domains took place, and more importantly, the surface was exclusively covered with CW nanowells after annealing. This result is interpreted in terms of Ostwald ripening which promotes the growth of CW domains consuming the unfavorable CCW domains. Annealing of the samples thus improved the efficiency of chiral induction. By careful inspection we also noticed that cDBA molecules with characteristic black edges were not included in the network after annealing, indicating that the homochiral surface was entirely composed of achiral DBA molecules. This observation implies desorption of **cDBA-OC12(*S*)** during the annealing step due to its lower adsorption energy relative to **DBA-OC12**.

Annealing experiment carried out with the 10 mol % **cDBA-OC12(*S*)/DBA-OC12** system at higher concentration (2.5×10^{-6} mol L^{-1}) resulted in a striking result of chirality reversal. Whereas at room temperature 81% of the surface was covered by CW nanowells, upon annealing at 80 °C, the system turned into a homochiral network of CCW nanowells which formed large domains due to ripening (Figures 32a and 32b). At intermediate concentrations, the system showed varying degree of chiral induction after annealing as shown in the histograms in Figure 32c. The monolayer obtained from an antipodal mixture of **cDBA-OC12(*R*)/DBA-OC12** gave rise to CW homochiral surface after annealing, confirming the reversal of the majority handedness under similar experimental conditions. As expected, in the absence of cDBA, the monolayer of **DBA-OC12** always remained globally racemic even after annealing.

In 2D crystal growth, initial nucleation is followed by free growth of the domains, which is terminated when the domains touch each other at the domain boundaries. Once the entire surface is covered with molecules, ripening starts between neighboring domains via a net flux of molecules from one domain to the other. The **cDBA-OC12(*S*)** molecules respond differently to the increase in the concentration and temperature. (1) They are incorporated in the CW network of **DBA-OC12** as sergeants at room temperature to define the chirality of the domain (Figures 28b and 28c). Upon annealing the handedness of the system is amplified via a ripening process. However, due to lower adsorption energy of **cDBA-OC12(*S*)** than that of **DBA-OC12**, the sergeant molecules are desorbed from the surface during the annealing process. (2) The **cDBA-OC12(*S*)** molecules occupy CCW nanowells preferentially as guests adopting a windmill-like conformation (Figures 29 and 30) to form stable host–guest complexes. Such enantioselective guest inclusion increases the relative stability of the CCW domains. The percentage of the **cDBA-OC12(*S*)** guests depends on the total solution concentration. At relatively high concentration, additional stabilization of the monolayer occurs via host–guest

complexation. Under such conditions, the more stable CCW domains containing **cDBA-OC12(*S*)** evolve by annealing via a ripening process to amplify the CCW nanowells, from which cDBA molecules are finally desorbed leaving the memory of the network structure. The fact that at the intermediate concentrations the system does not reach a homochiral surface (Figure 32c) is explained in terms of the relation between the rate of ripening and the length of domain boundaries. Namely, as ripening progresses, the rate of ripening decreases because of the decreasing domain boundaries due to increasing domain size. At a certain point, the ripening process reaches equilibrium, and the domain boundaries simply oscillate as was experimentally observed.

On the basis of the mechanistic considerations, we examined the control for the chirality amplification process, either by sergeant-and-soldier or host–guest mechanism, by molecular design of the inducer/guest molecules. As described before, **cDBA-OC12(*S*)-OC13(*R*)** serves as a more effective chirality inducer than **cDBA-OC12(*S*)** to induce the CW network with much smaller proportion. However, the **cDBA-OC12(*S*)OC13(*R*)/DBA-OC12** system (6% cDBA: 2.5×10^{-6} mol L^{-1}) did not show reversal of chirality upon annealing, because **cDBA-OC12(*S*)OC13(*R*)** did not serve as a guest in either CCW or CW nanowell. On the other hand, chirality amplification via the host–guest pathway was achieved by employing a combination of **cDBA-OC12(*S*)** and **DBA-OC10**. In this case, **cDBA-OC12(*S*)** cannot act as a sergeant due to its longer alkoxy chains. Sequential deposition of **DBA-OC10** (1.0×10^{-6} mol L^{-1}, 20 μL) followed by **cDBA-OC12(*S*)** (3.0×10^{-5} mol L^{-1}, 20 μL) at room temperature furnished equal surface coverage of the opposite-handed domains of **DBA-OC10** without any **cDBA-OC12(*S*)** sergeants, indicating lack of sergeant-and-soldiers effect. However, **cDBA-OC12(*S*)** molecules are adsorbed as guests preferentially in CCW nanowells. Annealing this system led to a CCW homochiral surface of **DBA-OC10** with considerable **cDBA-OC12(*S*)** guest molecules remaining adsorbed. These experiments using *different-sized guest* DBAs for the host–guest based chirality induction pathway confirms the high fidelity of the proposed mechanism.

5.4 Functionalization of Pore Interior. Host–guest recognition events, or molecular recognition in general, that take place in 3D space (i.e., solution, crystalline solid, liquid crystals, gels, membranes, and so on) are based on various noncovalent interactions including van der Waals force, hydrogen-bond, ion–dipole and dipole–dipole interactions.[71] In addition numerous host molecules that can change binding properties in response to external stimuli such as light irradiation and oxidation–reduction have been designed and synthesized to endow the host molecules with more sophisticated functions.[72] As described in section 5.1, the shallow nanowells formed by self-assembly of simple DBA molecules can be used as space for accommodating guest molecules which are adsorbed on the graphite surface by replacing the adsorbed solvent molecules, though the adsorption–desorption process is in principle dynamic with respect to the time-scale of STM measurement. Guest molecules are confined in the nanowell in a size- and shape-compatible manner via solely van der Waals interaction between the rim of the nanowells and the lateral periphery of the guest molecule(s). Taking into account the advances

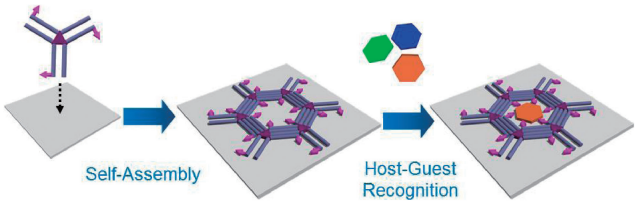

Figure 33. Schematic representation of on-surface host–guest binding in a functionalized nanowell formed by self-assembly of alternately functionalized DBA.

in host–guest chemistry in 3D space, it is obvious that the following challenges remain in pursuit in 2D space; (1) modification of the chemical environment of the 2D nanowells in a manner that guest binding takes place via non-covalent interactions other than van der Waals forces and (2) reversible modification of guest-accommodating properties of the nanowell in response to external stimuli. There are a few reports on the modification of 2D pores with space-controlling groups that recognize the size and shape of guest molecules.[17d,19] However, the construction of 2D pores equipped with functional groups capable of binding specific neutral guest molecules via polar noncovalent interactions has scarcely been achieved. No stimuli-responsive 2D pores that changes physical or chemical environment have been reported. We envisioned these objectives could be achieved by introducing appropriate functional groups at the end of three alternate alkyl chains of DBAs, called second-generation DBAs, as illustrated in Figure 33. Namely, the functional groups in second-generation DBAs represented by magenta arrows should be located at the outer positions of the interdigitation pair and the simple alkyl groups take the inner position because of steric reasons. This leads to the functional groups inevitably locating at the interior of the nanowells making them ready for guest binding. More importantly, selective introduction of different alkyl groups to the DBA core in an alternate fashion, one of the major issues in this molecular design, can be realized only by utilizing the synthetic protocol developed by us (Scheme 1).

First, construction of surface-confined pores lined with fluoroalkyl groups is described. We expected that such nanowells would selectively bind guest molecules by fluorophilicity and electrostatic interaction.[73] It is well known that homogeneous mixing of alkanes and fluoroalkanes is highly disfavored whereas fluorinated parts in molecules tend to aggregate by themselves due to a property known as fluorophilicity.[74] This unique behavior has been utilized as a key driving force in various supramolecular self-assemblies such as liquid crystalline materials and lipid bilayers, and host–guest complexes. In this respect, we designed and synthesized **DBA-F** having perfluoroalkyl groups at the end of the three alkoxy chains connected with *para*-phenylene linkers (Figure 34). As a reference compound, **DBA-H** having alkyl groups instead of the perfluoroalkyl groups was synthesized. We expected that both DBAs would form honeycomb structures in which the fluoroalkyl or alkyl groups are positioned around the perimeter of the hexagonal pores. To examine the guest binding abilities, we synthesized two complimentary guest molecules: hexakis-(phenylethynyl)benzene **HPEB** (Figure 16c) and its octadecafluoro derivative **HPEB-F** (Figure 34). These guest molecules

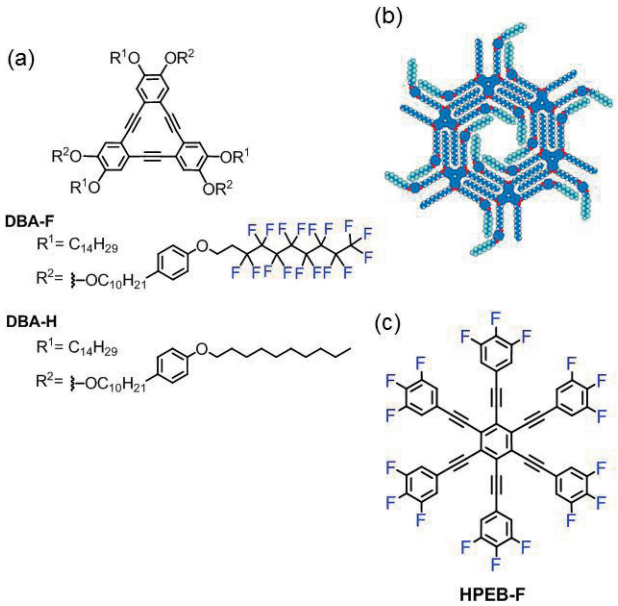

Figure 34. (a) Chemical structures of **DBA-F** and **DBA-H**, (b) a molecular model of the honeycomb structures formed by **DBA-F**, and (c) chemical structure of **HPEB-F**.

were chosen because of their shape and size that match the hexagonal pores of the DBAs in addition to the presence of 18 fluorine atoms furnished at the exterior edge of **HPEB-F**.

STM observations of monolayers formed by **DBA-F** and **DBA-H** at the PO/graphite interface, after annealing treatment at 70 °C for 30 min, revealed the formation of honeycomb structures in which the fluoroalkyl or alkyl groups are positioned around the perimeter of the hexagonal pores as expected (Figures 35a and 35b). The guest binding experiments were carried out at a constant DBA/guest mole ratio (= 2.4/1, total concentration: 4.4×10^{-6} mol L^{-1}) after optimization of conditions at which sensible comparison could be done. On the basis of the appearance of the pore space in the STM images, the pores are classified into three categories; *bright* pores containing immobilized guest, *fuzzy* pores with mobile guest, and *dark* pores without guest (Figures 35c–35f). Their distribution indicates that, whereas the host network of **DBA-F** accommodates both **HPEB-F** and **HPEB** efficiently, the host network of **DBA-H** exhibits marked selectivity with little affinities toward **HPEB-F** in contrast to high affinity to **HPEB**. On the basis of molecular mechanics calculations for the periodic host–guest complexes together with quantum chemical calculations for the model compounds to estimate interaction energies (representative models shown in Figures 35g and 35h), the strong host–guest affinity between **DBA-F** and **HPEB** guest is attributed to H···F electrostatic interactions between the peripheral hydrogen atoms of the guest and the fluoroalkyl groups of the 2D pores (Figures 35e and 35h). It should be emphasized that the host–guest pair of reverse relationship, **DBA-H** and **HPEB-F**, exhibited the least binding affinity (Figure 35d), which is ascribed to the *wrong* aromatic/aliphatic hydrogen/fluorine substitution patterns for electrostatic interaction. The moderate binding affinity between **DBA-F** and **HPEB-F** is understood in terms of compromise between fluorophilicity and the size of the DBA pore which is slightly too small to accommodate the guest (Figures 35c and 35g). Nevertheless, this is, to our knowledge, the first example of the use of such interactions in 2D guest binding. Unexpectedly, **DBA-H** and **HPEB** exhibits significant binding affinity in spite of weak interaction (only van der Waals force) and the slightly large pore size for the guest. In this case the dark or fuzzy pores are always surrounded by the bright pores each containing asterisk-shaped

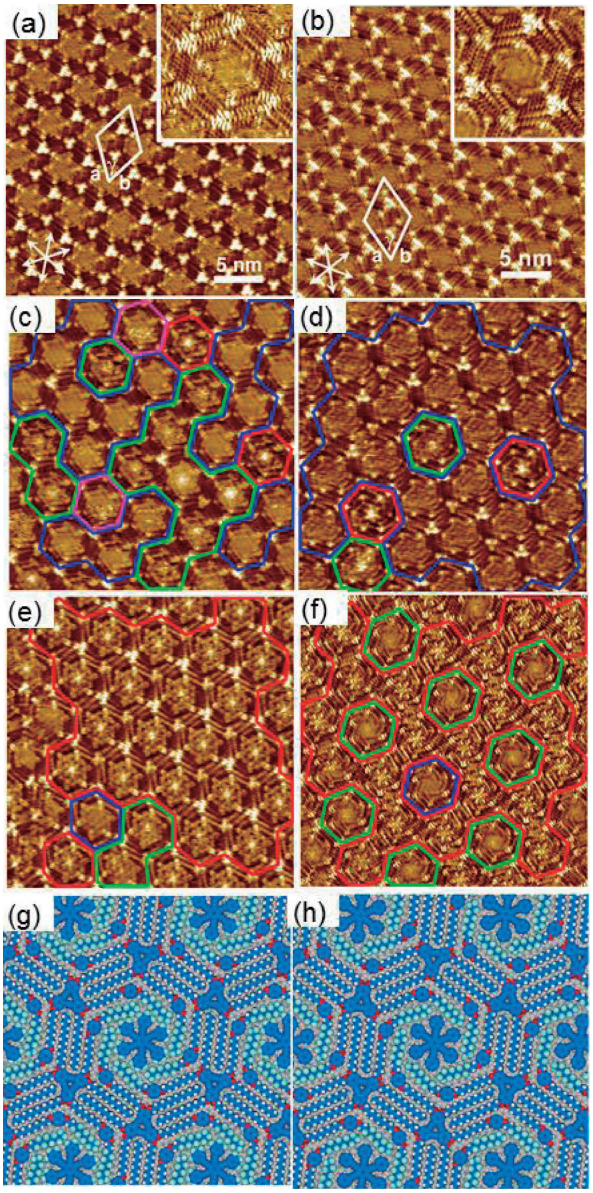

Figure 35. STM images of honeycomb structures of (a) **DBA-F** and (b) **DBA-H** formed at the PO/graphite interface. STM images of monolayers formed at the PO/graphite interface by (c) **DBA-F** and **HPEB-F**, (d) **DBA-H** and **HPEB-F**, (e) **DBA-F** and **HPEB**, and (f) **DBA-H** and **HPEB** with red, green, blue, and pink hexagons indicating the *bright pores*, *fuzzy pores*, *dark pores*, and pores which cannot be assigned, respectively. Tentative network models of (a) **DBA-F** and **HPEB-F** and (c) **DBA-F** and **HPEB** on a bilayered graphene sheet by molecular mechanics simulations. Reprinted with permission from Ref. 73. Copyright 2014 American Chemical Society.

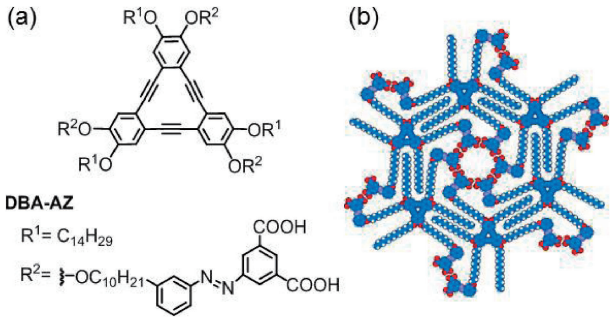

Figure 36. (a) Chemical structure of **DBA-AZ** and (b) a molecular model of the honeycomb structures formed by **DBA-AZ**. Reprinted with permission from Ref. 76. Copyright 2013 John Wiley and Sons.

feature (Figure 35f) indicating the formation of a superlattice structure. Moreover, careful inspection of the STM images revealed that the network pores containing the confined guest molecules are deformed to maximize van der Waals contact with the guest via an induced fit mechanism. This deformation occurs periodically leaving one pore surrounded by six guest-confined pores thus generating a superlattice structure. This represents another instance of superlattice formation induced by guest binding.[74]

Next, we investigated reversible modification of guest-accommodating properties of the nanowell in response to external stimuli. In this study the nanowell size was tailored so that it fits a specific guest molecule and can be changed reversibly by irradiation of different wavelength light. Though reversible modification of surface structures and functions using photochromic molecules such as azobenzene which are chemically or physically adsorbed at surfaces has been extensively studied,[75] this represents the first example of the construction of 2D pores which respond to external stimuli specifically at a single molecular level.

As a photoresponsive group we chose azobenzene on which two carboxy groups are introduced to create a confined space within a hydrogen-bonded cyclic hexamer of the isophthalic acid moieties, which is known to immobilize one coronene (**COR**: Figure 16c) molecule on surfaces via size and shape recognition (see Figures 18 and 19). On the basis of this design, **DBA-AZ** was synthesized. Here a *meta*-phenylene linker connected to a C12 alkyl chain was used to locate the cyclic hexamer of the dicarboxyazobenzene units at an appropriate direction in the pore (Figure 36).[76] We expected that the azobenzene units initially located on the surface in its planar *trans*-configuration would be desorbed from the surface after isomerization to the *cis*-configuration, thereby changing the pore size and shape significantly which can be assessed by the number of adsorbed **COR** guest molecules.

By drop casting an OA solution of **DAB-AZ** (1.0×10^{-5} mol L^{-1}) on graphite, the formation of a honeycomb network was observed as expected (Figure 37a). Nearly all azobenzene units direct toward the center of the nanowell, suggesting the formation of a cyclic hexamer of the dicarboxyazobenzene units by hydrogen bonds. Moreover, a solution of a photostationary mixture of **DBA-AZ** containing 57% of *cis*-azobenzene moieties formed mostly disordered structures together with

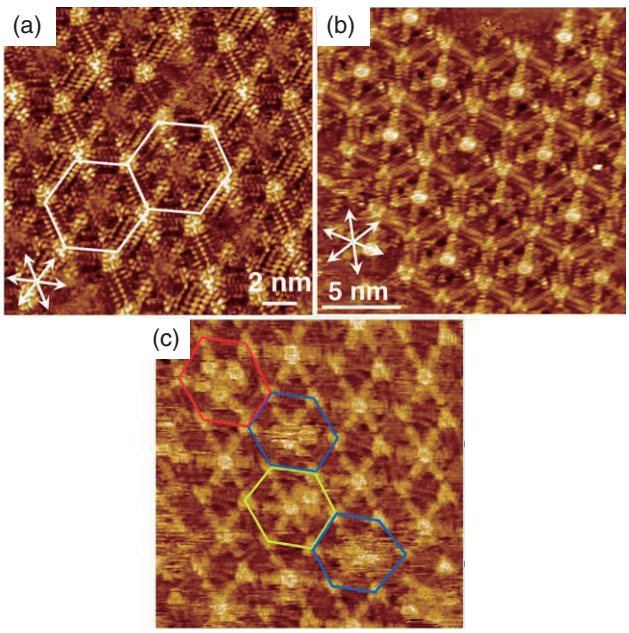

Figure 37. (a) A honeycomb structure formed by **DBA-AZ** at the OA/graphite interface. (b) A self-assembled monolayer formed from a mixture of **DBA-AZ** and excess **COR** at the OA/HOPG interface. (c) A self-assembled monolayer formed by in-situ UV irradiation of **DBA-AZ** at the OA/HOPG interface followed by addition of excess **COR**. The red, yellow, and blue hexagons indicate the pores containing four **COR**s, two **COR**s, and those with fuzzy images, respectively. Reprinted with permission from Ref. 76. Copyright 2013 John Wiley and Sons.

small honeycomb domains, confirming the importance of the *trans*-configuration for the formation of the hydrogen-bonded hexamer. Prior to irradiation, a saturated solution of **COR** in OA (5.5×10^{-4} mol L^{-1}) was dropped. As a result, single **COR** molecule was observed in 86% of the pores (Figure 37b); two **COR**s were found in 4% of the pores and 9% of the pores contained fuzzy feature. By irradiation of 320 nm light for 10 min followed by drop casting a saturated solution of **COR**, the number of the pores containing more than two **COR** molecules increased (Figure 37c). Statistical analysis revealed that 73% of the pores contain one **COR**, 16% two **COR**s, 3% three **COR**s, and 8% fuzzy features. Pores containing four **COR** molecules are also observed yet in small quantities (0.3%). When this mixture was irradiated with long-wavelength light ($\lambda > 400$ nm) for 10 min, the distribution of the number of **COR** molecules changed as follows: one **COR**, 92.3%; two **COR**s, 2.8%; fuzzy features, 4.8%. The recovery of the stoichiometric selectivity is attributed to the reduction of the pore size by *cis*-to-*trans* isomerization of the azobenzene units, demonstrating the reversibility of this process. Moreover, control experiments revealed that rapid diffusion and adsorption–desorption dynamics of **DBA-AZ** at the interface are unlikely, indicating that photoisomerization of the azobenzene units occurs while being adsorbed on the graphite surface.

With the success in the construction of tailored nanowells based on the formation of hydrogen-bonded hexamers of dicarboxyazobenzene units, we envisioned that this motif can be

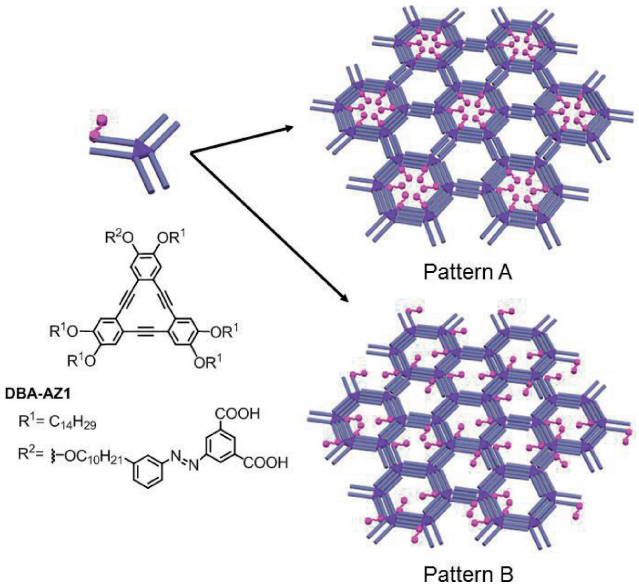

Figure 38. Schematic representation of periodically functionalized porous network (Pattern A) and randomly functionalized porous network (Pattern B) and chemical structure of **DBA-AZ1**. Reprinted with permission from Ref. 77. Copyright 2016 American Chemical Society.

used to construct periodically functionalized pores in the self-assembled 2D network of DBAs. To this end, **DBA-AZ1** bearing only one dicarboxyazobenzene unit was designed.[77] As shown in Figure 38, **DBA-AZ1** would assemble to form a Pattern A type network with periodically functionalized pores if the hydrogen bonds are efficient enough to bring all six carboxy groups into the same pore, whereas the formation of a Pattern B type network of random distribution would result otherwise. Periodically functionalized porous networks could be used for production of multi-component 2D architectures of high complexity by selective adsorption of guest molecules to the individual pores.

DBA-AZ1 was synthesized by the alkyne metathesis reaction of an unsymmetrical precursor having one dicarboxyazobenzene unit and five C14 alkyl chains using a Mo nitride complex. Monolayer formation was undertaken at the TCB/graphite interface at 2.1×10^{-6} mol L^{-1}. By deposition of the solution at room temperature, only small domains of a honeycomb structure were observed without any sign of the formation of cyclic hexamer of the isophthalic acid (Pattern B). On the other hand, by annealing treatment at 100 °C for 11 h, very large domains of the monolayer were formed (Figure 39a). As shown in Figure 39b, a honeycomb structure was formed. Some nanowells contain six dim spokes which correspond to the azobenzene units, indicating the formation of hydrogen-bonded cyclic hexamers of the isophthalic acid units. There are unfunctionalized nanowells without spoke-like features too. Notably, the locations of the two different type nanowells are periodically arranged within the honeycomb domain. Namely, the functionalized nanowells with small pore space were surrounded by large unfunctionalized nanowells exhibiting a long range periodicity. In the unfunctionalized nanowells there are occasionally bright fuzzy features, which we attribute to mobile self-adsorbed **DBA-AZ1** molecules. Our working hypothesis

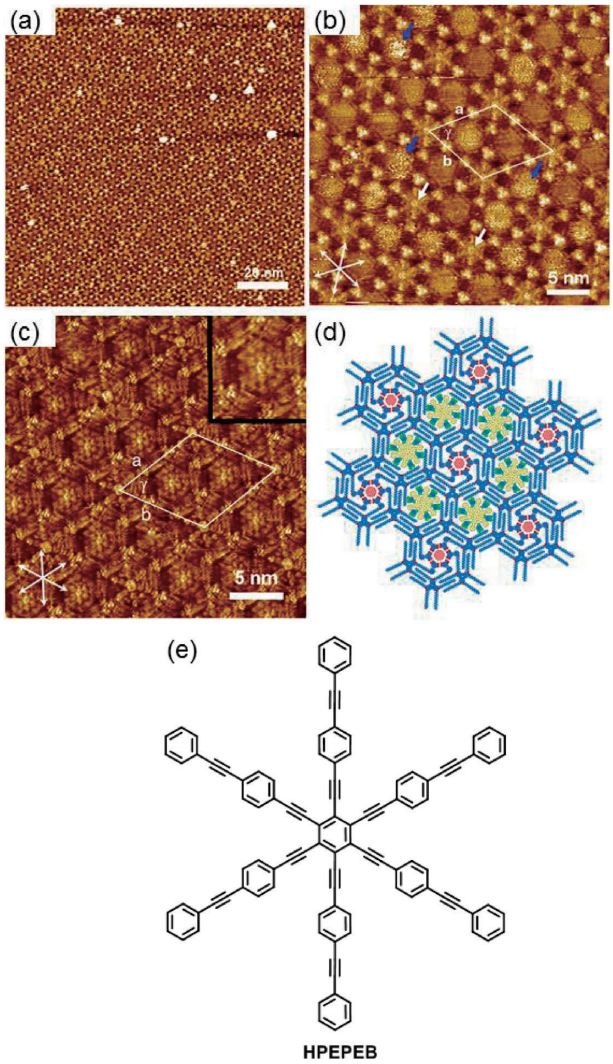

Figure 39. (a) STM image of monolayer of **DBA-AZ1** formed at the TCB/HOPG interface and (b) its enlarged image. The white arrows indicate the small pore formed by a hydrogen-bonded hexamer of isophthalic acid units and the blue arrows show fuzzy features in the unfunctionalized pores. (c) STM image of monolayer of a mixture of **DBA-AZ1**, **COR** and **HPEPEB** at the TCB/graphite interface. Inset shows a zoom-in image of the pore containing HPEPEB. (d) Molecular model of the three component monolayer. (e) Chemical structure of **HPEPEB**. Reprinted with permission from Ref. 77. Copyright 2016 American Chemical Society.

for construction of a periodic functionalization of the porous molecular network was thus experimentally verified.

To demonstrate use of a porous network with different-sized nanowells, the selective adsorption of two guest molecules, **COR** (Figure 16c) and **HPEPEB** (Figure 39e), in the porous network of **DBA-AZ1** was performed. The solute concentrations of each component were set to 1.7×10^{-6} mol L^{-1} for **DBA-AZ1**, 7.7×10^{-6} mol L^{-1} for **HPEPEB**, and 7.7×10^{-6} mol L^{-1} for **COR**, respectively, through optimization. Figure 39c shows an STM image of the monolayers prepared from the mixture at the TCB/graphite interface after annealing treatment at 100 °C for 11 h. Bright disks imaged at the center

of the bright spoke containing pores are due to **COR** molecules immobilized in the functionalized pores. Asterisk-like features consisting of dim dots visible at the large unfunctionalized nanowells are **HPEPEB** molecules. Close inspection of the large nanowells revealed co-adsorption of TCB molecules at the space between the "spokes" of radial **HPEPEB** molecule (Figure 39c inset). These observations reveal that a highly ordered three-component network was formed by selective adsorption of two different guest molecules at the respective nanowells in the periodically functionalized porous network (Figure 39d).

6. Conclusion

As described above, we found that DBAs formed porous 2D molecular networks of hexagonal lattices at liquid/solid interfaces via van der Waals interactions between interdigitated alkyl chains as the directional intermolecular linkages. We developed various aspects of on-surface self-assembly exploiting the unique features of DBA molecules, through fruitful international collaboration between Osaka and Leuven. The choice of DBA as a rigid core of the building blocks turned out to be crucial for the successful research that has lasted more than a decade, producing a lot of interesting results, many of which were never foreseen, due to excellent adaptivity as well as adaptability that the DBA molecules express. These include (i) pore size control by changing the alkoxy chain length, (ii) parity effect by using even or odd number alkoxy chains, (iii) generation of supramolecular chirality on surfaces by introducing stereocenters into the alkoxy chains, (iv) chemical modification of the pore interior for selective adsorption of guest molecules by introducing functional groups at the alkoxy chain terminals. It should be emphasized that the use of STM at the liquid/solid interface enabled us to gain information regarding how the molecules interact to each other to form highly ordered architecture on surfaces at a nearly atomic level precision. There are already a number of new issues evolved for further advances of this work such as chemical modification of graphene, on-surface reaction for the synthesis of 2D polymers which is a topic of intense current interest,[78] and epitaxial multilayer formation, to name just a few. For the chemical modification of graphene, the porous network of DBAs can be used as a mask; after modification at the pore space, the mask molecules can be removed to furnish periodically functionalized graphene, thereby making it possible to fine-tune semiconductor properties of modified graphene. The formation of stable dry films may find use for synthesis of 2D polymers, if we can introduce in the alkyl chains reactive functionalities which upon applying external stimuli connect the interdigitated alkyl chains. On the other hand, by introducing appropriate functionalities that would interact in vertical direction on the alkyl chains, it would be possible to form porous columns by growth of self-assembly to the vertical direction in addition to the network formed in lateral direction via van der Waals interaction. As such there remains a lot to be done in this field.

This work was supported by Grants-in-Aid for Scientific Research (Nos. 15H02164, 24350046, 21245012, 18205007). In Leuven, the fruitful collaboration with Osaka was made possible thanks to support from the Fund of Scientific Research-Flanders (FWO), Internal Funds KU Leuven, the Belgian Federal Science Policy Office (IAP-7/05) and funding from the European Research Council under the European Union's Seventh Framework Programme (FP7/2007–2013)/ERC grant agreement no. 340324. In addition, the collaboration was facilitated by JSPS and FWO under the Japan–Belgium Bilateral Joint Research Program. The authors are grateful to all people who contributed to this work and names are found in the references.

References

1 S. Laschat, A. Baro, N. Steinke, F. Giesselmann, C. Hägele, G. Scalia, R. Judele, E. Kapatsina, S. Sauer, A. Schreivogel, M. Tosoni, *Angew. Chem., Int. Ed.* **2007**, *46*, 4832.

2 P. Terech, R. G. Weiss, *Chem. Rev.* **1997**, *97*, 3133.

3 a) N. Sakai, R. Bhosale, D. Emery, J. Mareda, S. Matile, *J. Am. Chem. Soc.* **2010**, *132*, 6923. b) S. Günes, H. Neugebauer, N. S. Sariciftci, *Chem. Rev.* **2007**, *107*, 1324.

4 a) J. V. Barth, G. Costantini, K. Kern, *Nature* **2005**, *437*, 671. b) L. Bartels, *Nat. Chem.* **2010**, *2*, 87.

5 a) J. V. Barth, *Annu. Rev. Phys. Chem.* **2007**, *58*, 375. b) J. A. Theobald, N. S. Oxtoby, M. A. Phillips, N. R. Champness, P. H. Beton, *Nature* **2003**, *424*, 1029.

6 a) L. C. Giancarlo, G. W. Flynn, *Acc. Chem. Res.* **2000**, *33*, 491. b) P. Samorì, J. P. Rabe, *J. Phys.: Condens. Matter* **2002**, *14*, 9955. c) S. De Feyter, F. C. De Schryver, *J. Phys. Chem. B* **2005**, *109*, 4290. d) L.-J. Wan, *Acc. Chem. Res.* **2006**, *39*, 334. e) B. A. Hermann, L. J. Scherer, C. E. Housecroft, E. C. Constable, *Adv. Funct. Mater.* **2006**, *16*, 221. f) Y. Yang, C. Wang, *Chem. Soc. Rev.* **2009**, *38*, 2576.

7 a) K. E. Plass, A. L. Grzesiak, A. J. Matzger, *Acc. Chem. Res.* **2007**, *40*, 287. b) S. Furukawa, S. De Feyter, *Top. Curr. Chem.* **2009**, *287*, 87.

8 a) J. A. A. W. Elemans, S. Lei, S. De Feyter, *Angew. Chem., Int. Ed.* **2009**, *48*, 7298. b) D. Bonifazi, S. Mohnani, A. Llanes-Pallas, *Chem.—Eur. J.* **2009**, *15*, 7004. c) X. Ma, Y. Yang, K. Deng, Q. Zeng, K. Zhao, C. Wang, C. Bai, *J. Mater. Chem.* **2008**, *18*, 2074. d) T. Kudernac, S. Lei, J. A. A. W. Elemans, S. De Feyter, *Chem. Soc. Rev.* **2009**, *38*, 402. e) M. Surin, P. Samorì, *Small* **2007**, *3*, 190.

9 a) G. M. J. Schmidt, *Pure Appl. Chem.* **1971**, *27*, 647. b) G. R. Desiraju, *Crystal Engineering: The Design of Organic Solid*, Elsevier, Amsterdam, **1989**. c) G. R. Desiraju, *Angew. Chem., Int. Ed. Engl.* **1995**, *34*, 2311. d) N. Blagden, R. J. Davey, *Cryst. Growth Des.* **2003**, *3*, 873.

10 a) P. Samorì, *J. Mater. Chem.* **2004**, *14*, 1353. b) P. Samorì, *Chem. Soc. Rev.* **2005**, *34*, 551.

11 J. P. Rabe, S. Buchholz, *Science* **1991**, *253*, 424.

12 a) K. Tahara, S. Lei, J. Adisoejoso, S. De Feyter, Y. Tobe, *Chem. Commun.* **2010**, *46*, 8507. b) S. Lei, K. Tahara, J. Adisoejoso, T. Balandina, Y. Tobe, S. De Feyter, *CrystEngComm* **2010**, *12*, 3369.

13 a) M. Sonoda, Y. Sakai, T. Yoshimura, Y. Tobe, K. Kamada, *Chem. Lett.* **2004**, *33*, 972. b) T. Yoshimura, A. Inaba, M. Sonoda, K. Tahara, Y. Tobe, R. V. Williams, *Org. Lett.* **2006**, *8*, 2933. c) K. Tahara, T. Fujita, M. Sonoda, M. Shiro, Y. Tobe, *J. Am. Chem. Soc.* **2008**, *130*, 14339.

14 Y. Yang, C. Wang, *Curr. Opin. Colloid Interface Sci.* **2009**, *14*, 135.

15 K. G. Nath, O. Ivasenko, J. A. Miwa, H. Dang, J. D. Wuest, A. Nanci, D. F. Perepichka, F. Rosei, *J. Am. Chem. Soc.* **2006**, *128*,

4212.
16 a) R. Zacharia, H. Ulbricht, T. Hertel, *Phys. Rev. B* **2004**, *69*, 155406. b) K. Kim, K. E. Plass, A. J. Matzger, *Langmuir* **2003**, *19*, 7149. c) K. Kim, K. E. Plass, A. J. Matzger, *J. Am. Chem. Soc.* **2005**, *127*, 4879.
17 a) X. Zang, Q. Zeng, C. Wang, *Sci. China: Chem.* **2014**, *57*, 13. b) G. Schull, L. Douillard, C. Fiorini-Debuisschert, F. Charra, F. Mathevet, D. Kreher, A.-J. Attias, *Nano Lett.* **2006**, *6*, 1360. c) G. Schull, L. Douillard, C. Fiorini-Debuisschert, F. Charra, F. Mathevet, D. Kreher, A.-J. Attias, *Adv. Mater.* **2006**, *18*, 2954. d) S. Stepanow, M. Lingenfelder, A. Dmitriev, H. Spillmann, E. Delvigne, N. Lin, X. Deng, C. Cai, J. V. Barth, K. Kern, *Nat. Mater.* **2004**, *3*, 229. e) S. J. H. Griessl, M. Lackinger, F. Jamitzky, T. Markert, M. Hietschold, W. M. Heckl, *Langmuir* **2004**, *20*, 9403. f) G. Eder, S. Kloft, N. Martsinovich, K. Mahata, M. Schmittel, W. M. Heckl, M. Lackinger, *Langmuir* **2011**, *27*, 13563.
18 a) Y. Xue, M. B. Zimmt, *J. Am. Chem. Soc.* **2012**, *134*, 4503. b) Y.-T. Shen, M. Li, Y.-Y. Guo, K. Deng, Q.-D. Zeng, C. Wang, *Chem.—Asian J.* **2010**, *5*, 787.
19 a) L. M. A. Perdigão, A. Saywell, G. N. Fontes, P. A. Staniec, G. Goretzki, A. G. Phillips, N. R. Champness, P. H. Beton, *Chem.—Eur. J.* **2008**, *14*, 7600. b) A. G. Phillips, L. M. A. Perdigão, P. H. Beton, N. R. Champness, *Chem. Commun.* **2010**, *46*, 2775. c) M. T. Räisänen, A. G. Slater (née Phillips), N. R. Champness, M. Buck, *Chem. Sci.* **2012**, *3*, 84.
20 a) S. Furukawa, H. Uji-i, K. Tahara, T. Ichikawa, M. Sonoda, F. C. De Schryver, Y. Tobe, S. De Feyter, *J. Am. Chem. Soc.* **2006**, *128*, 3502. b) K. Tahara, S. Furukawa, H. Uji-i, T. Uchino, T. Ichikawa, J. Zhang, W. Mamdouh, M. Sonoda, F. C. De Schryver, S. De Feyter, Y. Tobe, *J. Am. Chem. Soc.* **2006**, *128*, 16613.
21 R. Lazzaroni, A. Calderone, G. Lambin, J. P. Rabe, J. L. Brédas, *Synth. Met.* **1991**, *41*, 525.
22 K. Tahara, S. Okuhata, J. Adisoejoso, S. Lei, T. Fujita, S. De Feyter, Y. Tobe, *J. Am. Chem. Soc.* **2009**, *131*, 17583.
23 S. Yin, C. Wang, X. Qiu, B. Xu, C. Bai, *Surf. Interface Anal.* **2001**, *32*, 248.
24 a) G. C. McGonigal, R. H. Bernhardt, D. J. Thomson, *Appl. Phys. Lett.* **1990**, *57*, 28. b) K. W. Herwig, B. Matthies, H. Taub, *Phys. Rev. Lett.* **1995**, *75*, 3154.
25 P. Wu, Q. Zeng, S. Xu, C. Wang, S. Yin, C.-L. Bai, *ChemPhysChem* **2001**, *2*, 750.
26 K. Tahara, C. A. Johnson, II, T. Fujita, M. Sonoda, F. C. De Schryver, S. De Feyter, M. M. Haley, Y. Tobe, *Langmuir* **2007**, *23*, 10190.
27 L. Xu, L. Yang, L. Cao, T. Li, S. Chen, D. Zhao, S. Lei, J. Ma, *Phys. Chem. Chem. Phys.* **2013**, *15*, 11748.
28 a) F. Charra, J. Cousty, *Phys. Rev. Lett.* **1998**, *80*, 1682. b) S. Xu, Q. Zeng, J. Lu, C. Wang, L. Wan, C.-L. Bai, *Surf. Sci.* **2003**, *538*, L451. c) C. Arrigoni, G. Schull, D. Bléger, L. Douillard, C. Fiorini-Debuisschert, F. Mathevet, D. Kreher, A.-J. Attias, F. Charra, *J. Phys. Chem. Lett.* **2010**, *1*, 190.
29 a) K. Tahara, M. L. Abraham, K. Igawa, K. Katayama, I. M. Oppel, Y. Tobe, *Chem. Commun.* **2014**, *50*, 7683. b) S. Yokoyama, T. Hirose, K. Matsuda, *Langmuir* **2015**, *31*, 6404.
30 S. Lei, K. Tahara, F. C. De Schryver, M. Van der Auweraer, Y. Tobe, S. De Feyter, *Angew. Chem., Int. Ed.* **2008**, *47*, 2964.
31 K. Tahara, S. Lei, D. Mössinger, H. Kozuma, K. Inukai, M. Van der Auweraer, F. C. De Schryver, S. Höger, Y. Tobe, S. De Feyter, *Chem. Commun.* **2008**, *44*, 3897.
32 K. Tahara, J. Adisoejoso, K. Inukai, S. Lei, A. Noguchi, B. Li, W. Vanderlinden, S. De Feyter, Y. Tobe, *Chem. Commun.* **2014**, *50*, 2831.
33 a) S. Berner, M. de Wild, L. Ramoino, S. Ivan, A. Baratoff, H.-J. Güntherodt, H. Suzuki, D. Schlettwein, T. A. Jung, *Phys. Rev. B* **2003**, *68*, 115410. b) M. Roos, H. E. Hoster, A. Breitruck, R. J. Behm, *Phys. Chem. Chem. Phys.* **2007**, *9*, 5672. c) F. Vidal, E. Delvigne, S. Stepanow, N. Lin, J. V. Barth, K. Kern, *J. Am. Chem. Soc.* **2005**, *127*, 10101. d) M. Stöhr, M. Wahl, C. H. Galka, T. Riehm, T. A. Jung, L. H. Gade, *Angew. Chem., Int. Ed.* **2005**, *44*, 7394.
34 a) L. Kampschulte, T. L. Werblowsky, R. S. K. Kishore, M. Schmittel, W. M. Heckl, M. Lackinger, *J. Am. Chem. Soc.* **2008**, *130*, 8502. b) R. Gutzler, T. Sirtl, J. F. Dienstmaier, K. Mahata, W. M. Heckel, M. Schmittel, M. Lackinger, *J. Am. Chem. Soc.* **2010**, *132*, 5084. c) C. Meier, M. Roos, D. Künzel, A. Breitruck, H. E. Hoster, K. Landfester, A. Gross, R. J. Behm, U. Ziener, *J. Phys. Chem. C* **2010**, *114*, 1268. d) C.-A. Palma, J. Bjork, M. Bonini, M. S. Dyer, A. Llanes-Pallas, D. Bonifazi, M. Persson, P. Samorì, *J. Am. Chem. Soc.* **2009**, *131*, 13062.
35 C.-A. Palma, M. Bonini, T. Breiner, P. Samorì, *Adv. Mater.* **2009**, *21*, 1383.
36 a) C. Marie, F. Silly, L. Tortech, K. Müllen, D. Fichou, *ACS Nano* **2010**, *4*, 1288. b) J. Saiz-Poseu, J. Faraudo, A. Figueras, R. Alibes, F. Busqué, D. Ruiz-Molina, *Chem.—Eur. J.* **2012**, *18*, 3056. c) Y. Li, C. Liu, Y. Xie, X. Li, X. Li, X. Fan, K. Deng, Q. Zeng, C. Wang, *Phys. Chem. Chem. Phys.* **2013**, *15*, 125. d) C.-J. Li, Q.-D. Zeng, Y.-H. Liu, L.-J. Wan, C. Wang, C.-R. Wang, C.-L. Bai, *ChemPhysChem* **2003**, *4*, 857. e) Y.-T. Shen, N. Zhu, X.-M. Zhang, K. Deng, W. Feng, Q. Yan, S. Lei, D. Zhao, Q.-D. Zeng, C. Wang, *Chem.—Eur. J.* **2011**, *17*, 7061. f) J. Adisoejoso, K. Tahara, S. Lei, P. Szabelski, W. Rżysko, K. Inukai, M. O. Blunt, Y. Tobe, S. De Feyter, *ACS Nano* **2012**, *6*, 897. g) A. Jahanbekam, S. Vorpahl, U. Mazur, K. W. Hipps, *J. Phys. Chem. C* **2013**, *117*, 2914.
37 a) A. Bellec, C. Arrigoni, G. Schull, L. Douillard, C. Fiorini-Debuisschert, F. Mathevet, D. Kreher, A.-J. Attias, F. Charra, *J. Chem. Phys.* **2011**, *134*, 124702. b) S. Ahn, A. J. Matzger, *J. Am. Chem. Soc.* **2010**, *132*, 11364. c) L. Kampschulte, T. L. Werblowsky, R. S. Kishore, M. Schmittel, W. M. Heckl, M. Lackinger, *J. Am. Chem. Soc.* **2008**, *130*, 8502.
38 M. O. Blunt, J. Adisoejoso, K. Tahara, K. Katayama, M. Van der Auweraer, Y. Tobe, S. De Feyter, *J. Am. Chem. Soc.* **2013**, *135*, 12068.
39 a) A. Stabel, R. Heinz, F. C. De Schryver, J. P. Rabe, *J. Phys. Chem.* **1995**, *99*, 505. b) M. Lackinger, S. Griessl, L. Kampschulte, F. Jamitzky, W. M. Heckl, *Small* **2005**, *1*, 532.
40 M. Mammen, E. I. Shakhnovich, J. M. Deutch, G. M. Whitesides, *J. Org. Chem.* **1998**, *63*, 3821.
41 K. Tahara, K. Kaneko, K. Katayama, S. Itano, C. H. Nguyen, D. D. D. Amorim, S. De Feyter, Y. Tobe, *Langmuir* **2015**, *31*, 7032.
42 a) W. J. Yu, L. Liao, S. H. Chae, Y. H. Lee, X. Duan, *Nano Lett.* **2011**, *11*, 4759. b) B. N. Szafranek, D. Schall, M. Otto, D. Neumaier, H. Kurz, *Nano Lett.* **2011**, *11*, 2640. c) M. C. Prado, R. Nascimento, L. G. Moura, M. J. S. Matos, M. S. C. Mazzoni, L. G. Cancado, H. Chacham, B. R. A. Neves, *ACS Nano* **2011**, *5*, 394. d) X. Dong, Y. Shi, Y. Zhao, D. Chen, J. Ye, Y. Yao, F. Gao, Z. Ni, T. Yu, Z. Shen, Y. Huang, P. Chen, L.-J. Li, *Phys. Rev. Lett.* **2009**, *102*, 135501. e) V. Georgakilas, M. Otyepka, A. B. Bourlinos, V. Chandra, N. Kim, K. C. Kemp, P. Hobza, R. Zboril, K. S. Kim, *Chem. Rev.* **2012**, *112*, 6156.
43 a) Q. H. Wang, M. C. Hersam, *Nano Lett.* **2011**, *11*, 589. b) A. J. Pollard, E. W. Perkins, N. A. Smith, A. Saywell, G.

Goretzki, A. G. Phillips, S. P. Argent, H. Sachdev, F. Müller, S. Hüfner, S. Gsell, M. Fischer, M. Schreck, J. Osterwalder, T. Greber, S. Berner, N. R. Champness, P. H. Beton, *Angew. Chem., Int. Ed.* **2010**, *49*, 1794. c) K. Xiao, W. Deng, J. K. Keum, M. Yoon, I. V. Vlassiouk, K. W. Clark, A.-P. Li, I. I. Kravchenko, G. Gu, E. A. Payzant, B. G. Sumpter, S. C. Smith, J. F. Browning, D. B. Geohegan, *J. Am. Chem. Soc.* **2013**, *135*, 3680. d) Y. Ogawa, T. Niu, S. L. Wong, M. Tsuji, A. T. S. Wee, W. Chen, H. Ago, *J. Phys. Chem. C* **2013**, *117*, 21849. e) P. Järvinen, S. K. Hämäläinen, K. Banerjee, P. Häkkinen, M. Ijäs, A. Harju, P. Liljeroth, *Nano Lett.* **2013**, *13*, 3199.

44 B. Li, K. Tahara, J. Adisoejoso, W. Vanderlinden, K. S. Mali, S. De Gendt, Y. Tobe, S. De Feyter, *ACS Nano* **2013**, *7*, 10764.

45 a) N. Katsonis, A. Marchenko, D. Fichou, *J. Am. Chem. Soc.* **2003**, *125*, 13682. b) T. Kudernac, N. Sändig, T. F. Landaluce, B. J. van Wees, P. Rudolf, N. Katsonis, F. Zerbetto, B. L. Feringa, *J. Am. Chem. Soc.* **2009**, *131*, 15655. c) Z. X. Xie, X. Xu, B. W. Mao, K. Tanaka, *Langmuir* **2002**, *18*, 3113.

46 T. Balandina, K. Tahara, N. Sändig, M. Blunt, J. Adisoejoso, S. Lei, F. Zerbetto, Y. Tobe, S. De Feyter, *ACS Nano* **2012**, *6*, 8381.

47 By collaboration with the group of Profs. Kim and Kawai, we also investigated self-assembly of unsubstituted DBA, **DBA-OC1** and **DBA-OC4** on Au(111) under UHV conditions, where geometry of self-assembly is dominated by epitaxial effect, hydrogen bonding, and/or van der Waals interactions depending on the substituents. a) J.-H. Kim, K. Tahara, J. Jung, S. De Feyter, Y. Tobe, Y. Kim, M. Kawai, *J. Phys. Chem. C* **2012**, *116*, 17082. b) J.-H. Kim, J. Jung, K. Tahara, Y. Tobe, Y. Kim, M. Kawai, *J. Chem. Phys.* **2014**, *140*, 074709.

48 S. Furukawa, K. Tahara, F. C. De Schryver, M. Van der Auweraer, Y. Tobe, S. De Feyter, *Angew. Chem., Int. Ed.* **2007**, *46*, 2831.

49 X. Feng, J. Wu, M. Ai, W. Pisula, L. Zhi, J. P. Rabe, K. Müllen, *Angew. Chem., Int. Ed.* **2007**, *46*, 3033.

50 S. Lei, K. Tahara, X. Feng, S. Furukawa, F. C. De Schryver, K. Müllen, Y. Tobe, S. De Feyter, *J. Am. Chem. Soc.* **2008**, *130*, 7119.

51 a) D. Mössinger, J. Hornung, S. Lei, S. De Feyter, S. Höger, *Angew. Chem., Int. Ed.* **2007**, *46*, 6802. b) J. A. Theobald, N. S. Oxtoby, N. R. Champness, P. H. Beton, T. J. S. Dennis, *Langmuir* **2005**, *21*, 2038. c) X.-H. Kong, K. Deng, Y.-L. Yang, Q.-D. Zeng, C. Wang, *J. Phys. Chem. C* **2007**, *111*, 9235.

52 S. Lei, M. Surin, K. Tahara, J. Adisoejoso, R. Lazzaroni, Y. Tobe, S. De Feyter, *Nano Lett.* **2008**, *8*, 2541.

53 J. Adisoejoso, K. Tahara, S. Okuhata, S. Lei, Y. Tobe, S. De Feyter, *Angew. Chem., Int. Ed.* **2009**, *48*, 7353.

54 a) L. Ramin, A. Jabbarzadeh, *Langmuir* **2011**, *27*, 9748. b) X. Liu, T. Wang, M. Liu, *Langmuir* **2012**, *28*, 3474. c) N. Nerngchamnong, L. Yuan, D.-C. Qi, J. Li, D. Thompson, C. A. Nijhuis, *Nat. Nanotechnol.* **2013**, *8*, 113. d) F. Tao, S. L. Bernasek, *Chem. Rev.* **2007**, *107*, 1408. e) L. Xu, X. Miao, B. Zha, W. Deng, *Chem.—Asian J.* **2013**, *8*, 926.

55 a) L. Messe, S. M. Clarke, C. Dong, R. K. Thomas, A. Inaba, M. D. Alba, M. A. Castro, *Langmuir* **2002**, *18*, 9429. b) G. Wang, S. Lei, S. De Feyter, R. Feldman, J. E. Parker, S. M. Clarke, *Langmuir* **2008**, *24*, 2501.

56 S. M. Clarke, L. Messe, J. Adams, A. Inaba, T. Arnold, R. K. Thomas, *Chem. Phys. Lett.* **2003**, *373*, 480.

57 E. Ghijsens, O. Ivasenko, K. Tahara, H. Yamaga, S. Itano, T. Balandina, Y. Tobe, S. De Feyter, *ACS Nano* **2013**, *7*, 8031.

58 a) H. Spillmann, A. Dmitriev, N. Lin, P. Messina, J. V. Barth, K. Kern, *J. Am. Chem. Soc.* **2003**, *125*, 10725. b) W. Xiao, X. Feng, P. Ruffieux, O. Gröning, K. Müllen, R. Fasel, *J. Am. Chem. Soc.* **2008**, *130*, 8911. c) J. Liu, T. Chen, X. Deng, D. Wang, J. Pei, L.-J. Wan, *J. Am. Chem. Soc.* **2011**, *133*, 21010. d) S.-S. Jester, E. Sigmund, L. M. Röck, S. Höger, *Angew. Chem., Int. Ed.* **2012**, *51*, 8555.

59 S. Lei, K. Tahara, K. Müllen, P. Szabelski, Y. Tobe, S. De Feyter, *ACS Nano* **2011**, *5*, 4145.

60 J. Adisoejoso, K. Tahara, S. Lei, P. Szabelski, W. Rżysko, K. Inukai, M. O. Blunt, Y. Tobe, S. De Feyter, *ACS Nano* **2012**, *6*, 897.

61 Reviews: a) R. Raval, *Chem. Soc. Rev.* **2009**, *38*, 707. b) K.-H. Ernst, *Z. Phys. Chem.* **2009**, *223*, 37.

62 For molecular chirality: a) M. Böhringer, W.-D. Schneider, R. Berndt, *Angew. Chem., Int. Ed.* **2000**, *39*, 792. b) C. B. France, B. A. Parkinson, *J. Am. Chem. Soc.* **2003**, *125*, 12712. c) R. Cortés, A. Mascaraque, P. Schmidt-Weber, H. Dil, T. U. Kampen, K. Horn, *Nano Lett.* **2008**, *8*, 4162. d) J. Zhang, B. Lin, X. Cui, B. Wang, J. Yang, J. G. Hou, *J. Am. Chem. Soc.* **2009**, *131*, 5885. e) B. Yang, Y. Wang, H. Cun, S. Du, M. Xu, Y. Wang, K.-H. Ernst, H.-J. Gao, *J. Am. Chem. Soc.* **2010**, *132*, 10440. f) T. Tsuya, K. Iritani, K. Tahara, Y. Tobe, T. Iwanaga, S. Toyota, *Chem.—Eur. J.* **2015**, *21*, 5520.

63 For supramolecular chirality: a) F. Vidal, E. Delvigne, S. Stepanow, N. Lin, J. V. Barth, K. Kern, *J. Am. Chem. Soc.* **2005**, *127*, 10101. b) M. Schöck, R. Otero, S. Stojkovic, F. Hümmelink, A. Gourdon, E. Lægsgaard, I. Stensgaard, C. Joachim, F. Besenbacher, *J. Phys. Chem. B* **2006**, *110*, 12835. c) S. Weigelt, C. Busse, L. Petersen, E. Rauls, B. Hammer, K. V. Gothelf, F. Besenbacher, T. R. Linderoth, *Nat. Mater.* **2006**, *5*, 112. d) P. Donovan, A. Robin, M. S. Dyer, M. Persson, R. Raval, *Chem.—Eur. J.* **2010**, *16*, 11641.

64 For chirality induction: a) M. Parschau, S. Romer, K.-H. Ernst, *J. Am. Chem. Soc.* **2004**, *126*, 15398. b) R. Fasel, M. Parschau, K.-H. Ernst, *Nature* **2006**, *439*, 449. c) S. Haq, N. Liu, V. Humblot, A. P. J. Jansen, R. Raval, *Nat. Chem.* **2009**, *1*, 409. d) F. Masini, N. Kalashnyk, M. M. Knudsen, J. R. Cramer, E. Lægsgaard, F. Besenbacher, K. V. Gothelf, T. R. Linderoth, *J. Am. Chem. Soc.* **2011**, *133*, 13910.

65 a) M. M. Green, N. C. Peterson, T. Sato, A. Teramoto, R. Cook, S. Lifson, *Science* **1995**, *268*, 1860. b) A. R. A. Palmans, J. A. J. M. Vekemans, E. E. Havinga, E. W. Meijer, *Angew. Chem., Int. Ed. Engl.* **1997**, *36*, 2648. c) J. H. K. K. Hirschberg, L. Brunsveld, A. Ramzi, J. A. J. M. Vekemans, R. P. Sijbesma, E. W. Maijer, *Nature* **2000**, *407*, 170.

66 K. Tahara, H. Yamaga, E. Ghijsens, K. Inukai, J. Adisoejoso, M. O. Blunt, S. De Feyter, Y. Tobe, *Nat. Chem.* **2011**, *3*, 714; See also: K. Tahara, H. Yamaga, E. Ghijsens, K. Inukai, J. Adisoejoso, M. O. Blunt, S. De Feyter, Y. Tobe, *Nat. Chem.* **2014**, *6*, 1024.

67 We also found chirality induction of the porous networks of DBAs by using chiral solvents: I. Destoop, E. Ghijsens, K. Katayama, K. Tahara, K. S. Mali, Y. Tobe, S. De Feyter, *J. Am. Chem. Soc.* **2012**, *134*, 19568.

68 E. Ghijsens, H. Cao, A. Noguchi, O. Ivasenko, Y. Fang, K. Tahara, Y. Tobe, S. De Feyter, *Chem. Commun.* **2015**, *51*, 4766.

69 E. Ghijsens, J. Adisoejoso, H. Van Gorp, I. Destoop, A. Noguchi, O. Ivasenko, K. Tahara, M. Van der Auweraer, Y. Tobe, S. De Feyter, *J. Chem. Phys.* **2015**, *142*, 101932.

70 Y. Fang, E. Ghijsens, O. Ivasenko, H. Cao, A. Noguchi, K. S. Mali, K. Tahara, Y. Tobe, S. De Feyter, *Nat. Chem.* **2016**, *8*,

711.
71 a) J.-M. Lehn, *Supramolecular Chemistry*, Wiley-VCH, Weinheim, **1995**. doi:10.1002/3527607439. b) F. Zeng, S. C. Zimmerman, *Chem. Rev.* **1997**, *97*, 1681. c) E. V. Anslyn, D. A. Dougherty, *Modern Physical Organic Chemistry*, University Science Books, Sausalito, **2006**, Chap. 4.
72 a) *Molecular Devices and Machines*, ed. by V. Balzani, M. Venturi, A. Credi, Wiley-VCH, Weinheim, **2003**. doi:10.1002/3527601600. b) D. Philp, J. F. Stoddart, *Angew. Chem., Int. Ed. Engl.* **1996**, *35*, 1154. c) J. A. A. W. Elemans, A. E. Rowan, R. J. M. Nolte, *J. Mater. Chem.* **2003**, *13*, 2661. d) T. Aida, E. W. Meijer, S. I. Stupp, *Science* **2012**, *335*, 813.
73 K. Tahara, K. Katayama, M. O. Blunt, K. Iritani, S. De Feyter, Y. Tobe, *ACS Nano* **2014**, *8*, 8683.
74 M. P. Krafft, J. G. Riess, *Chem. Rev.* **2009**, *109*, 1714.
75 W. R. Browne, B. L. Feringa, *Annu. Rev. Phys. Chem.* **2009**, *60*, 407.
76 K. Tahara, K. Inukai, J. Adisoejoso, H. Yamaga, T. Balandina, M. O. Blunt, S. De Feyter, Y. Tobe, *Angew. Chem., Int. Ed.* **2013**, *52*, 8373.
77 K. Tahara, K. Nakatani, K. Iritani, S. De Feyter, Y. Tobe, *ACS Nano* **2016**, *10*, 2113.
78 a) J. Sakamoto, J. van Heijst, O. Lukin, A. D. Schlüter, *Angew. Chem., Int. Ed.* **2009**, *48*, 1030. b) X. Zhuang, Y. Mai, D. Wu, F. Zhang, X. Feng, *Adv. Mater.* **2015**, *27*, 403. c) Q. Fan, J. M. Gottfried, J. Zhu, *Acc. Chem. Res.* **2015**, *48*, 2484. d) P. Payamyar, B. T. King, H. C. Öttinger, A. D. Schlüter, *Chem. Commun.* **2016**, *52*, 18.